CHAPTER 1

INTRODUCTION

1.1 GENERAL BACKGROUND

Most metals are stable only under reducing conditions and corrode upon exposure to an oxidizing environment. Metals producers combat this problem in various ways. Steel producers use various organic and inorganic coatings to protect cold-rolled steel (CRS) sheets from corrosion during shipment and storage. Some coatings are designed to retard corrosion by control of the electrochemistry, while others such as conversion and organic coatings create physical barriers to retard the corrosion rate in an oxidizing environment.

Traditionally, conversion coatings are produced by exposing CRS sheets to phosphoric acid (*phosphating process*) or chromic acid (*chromating process*) or both (Wiederholt, 1965). The latter provides more effective corrosion protection. However, the chromate salts used in metals industry as corrosion inhibitor are carcinogenic, create skin rashes and cause other environmental problems. Because of its toxicity, the Environmental Protection Agency (EPA) of the U.S. and similar agencies in other countries are empowered to take appropriate legislative measures against the use of chromium. In the UK, the occupational exposure limit (OEL) is 0.05 mg/m^3 for Cr (VI) ions and 0.5 mg/m^3 for Cr (III) (Brown, 1996). In some countries, the use of lead and chromium is banned for paint and other coating purposes. Other countries will soon follow the suit. The Global Environmental Facility (GEF) of the World Bank is taking measures to minimize environmental problems such as destruction of the ozone layer and smog problems created by the use of volatile solvents used in coatings industry.

Serious environmental and health concerns about the chromating process have generated a great deal of interest in developing chrome-free conversion coatings. Most new developments are based on organic coatings, which can also protect steel from fingerprints that act as seats for corrosion. Another function of conversion coatings is to provide good paint adhesion to topcoats.

Of the various organic conversion coatings being developed, perhaps the silane-coupling agents have received the most attention. These reagents are capable of forming strong bonds to metal substrates and, at the same time, of forming cross-linking polymers on the surface, both of

which contribute to producing good corrosion protection. Furthermore, proper choice of the terminal groups of the silane coupling agents can improve the adhesion of organic topcoats. Most methods of using silanes for conversion coating applications are protected by patents. Recent publications claim that the conversion coatings formed by silane coupling agents are comparable to or better than the chrome conversion coatings and can provide excellent seats for paint adhesion (Child, 1999; Mittal, 2001; Plueddemann, 1991; Tang, 1997; Puomi, 2001; Van Ooij, 1998c and 2003).

Schulman and Bouman (1997) used long-chain carboxylic acids as organic seals for anodized aluminum. Salt spray tests showed that its corrosion resistance was superior to that obtained by chromates. The organic seals exhibited the healing capacity that is provided by chromates. The authors suggested that the same technique can be used for steel, if it is coated with aluminum, anodized, and sealed with the fatty acids. On the other hand, Hefter, et al. (1997) reported that straight chain carboxylates could be used directly as organic corrosion inhibitors for steel, copper and aluminum.

Sulfur compounds have a strong affinity for transition metal surfaces. They can form strongly bonded, well ordered, and dense *self-assembled monolayers* (SAMs) on metal surfaces. A film of the SAM may act as an excellent barrier for corrosion protection of metal substrates. Jennings, et al. (1996, 1998) studied the SAMs of alkanethiols with long carbon chains (C_{18} and C_{22}) on copper to provide corrosion resistance in aqueous environments. They used evaporated copper films on silicon wafers as substrates and measured water contact angles over the organic coatings. It was suggested that the monolayer films provided a barrier against water penetration. The corrosion rate of copper varies with the film thickness, which further depends on chain length. In order to increase the thickness, they tried to construct a multilayer assembly on the copper surface. Mercaptoalcohol ($HS(CH_2)_nOH$, n=11, 22) was used for the first layer, and an alkyltrichlorosilane ($CH_3(CH_2)_{17}SiCl_3$) for the second layer through the reaction between the hydroxyl group and siloxane. It was found, however, that the bilayer films were not effective in improving the corrosion resistance.

A process for producing a chromium-free conversion coating for aluminum and steel was developed by McIntyre, et al. (1997). In this process, a metal substrate was contacted with a reagent prior to the application of a polymer topcoat. It produced a film of about 20~30 nm in thickness, which was referred to as a reactive conversion organic coating (ROCC). The film was

composed of an inorganic inner layer and an outer organic layer. The organic portion is highly functionalized, which aids in improving the adhesion of organic topcoats. The authors noted that the ROCC-treated steel, topcoated with various systems, was comparable to iron phosphate treated substrates with chromate seals. The reagent contains no toxic metals, and the organic portion of the film is biodegradable. However, the authors did not disclose the nature of the reagent. The process of producing ROCC uses equipment and conditions that are similar to those used in phosphating operations.

A new chromium-free organic-inorganic composite coated steel sheet has been developed in Japan. This product consists of a thin composite coating on galvanized steel sheet. It can provide the excellent corrosion resistance comparable to chromate-coated steel sheet and has a good balance of corrosion resistance, conductivity, weldability, anti-fingerprint property, and paint adhesion (Kubota, 2000).

In the steel industry, the primary means of corrosion inhibition include galvanizing (with zinc and zinc-nickel coatings) and organic topcoats. Epoxy ester, polyurethane, acrylics, and silicon resins are used as topcoats for the steel sheets that are used for manufacturing inner and outer panels of automobiles. Epoxy coatings bond strongly to substrates, and are resistant to impact, heat, and abrasion. Acrylic resins are resistant to UV, but are relatively weak to chemical attacks. Silicone resins, on the other hand, produce hard, tough, and heat-resistant coatings. Thus, a combination of these and other resins can produce organic coatings with desirable physical and chemical characteristics as well as corrosion resistance. In general, the requirements for steel sheets to be used for automobile panels are substantially higher than those used for household, office, and computer appliances (e.g., CD-ROM cases, copy machine panels, and refrigerator panels). For the latter applications, however, it is necessary that the steel sheets with organic coatings have anti-fingerprint capabilities. Otherwise, the area of a steel sheet where fingerprints are located may become the nuclei of corrosion due to the moisture and salt secreted by humans.

This three-year R&D project, funded by Pohang Iron & Steel Co., Ltd. (POSCO), Korea, aims to develop environmentally friendly non-chrome conversion coatings for cold-rolled steel sheets. During the first two-year period, three novel coating systems were developed with satisfactory corrosion resistance: i) carboxylic acids coatings on phosphated EG steel sheets; ii) an alkanethiol monolayer coating with nanoscale thickness on both phosphated EG and

Electrogalvanized (EG) steel sheets; and iii) thiol-modified resin coatings in micron-scale thickness on EG steel sheets. These novel coatings will be introduced in the coming chapters.

1.2 LITERATURE REVIEW

1.2.1 Corrosion Protection of Metals by Organic Coatings

1.2.1.1 General Information

Protective coatings represent the most widely used method of corrosion control of metal substrates under various corrosive conditions from atmospheric exposure to full immersion into strongly corrosive solutions. A protection coating is actually a film separating two highly reactive materials, i.e., metal and corrosive media. This film primarily acts as a physical barrier between the two to provide resistance to the diffusion of water, water vapor, oxygen and other corrosive media, so that corrosion of metal substrates is retarded.

Protective coatings can be loosely categorized into metallic coatings, nonmetallic inorganic coatings, and organic coatings, although, there is some overlap. Conventional organic coatings consist of binder, pigments and fillers, additives, and solvents. The corrosion protection provided by organic coatings results either from the barrier action of the layer or from the active corrosion inhibition of pigments in the coating. Paints are an example of organic protective coatings, which also play a decorative role. On the other hand, an organic conversion coating is an organic thin film formed on metal substrates to promote corrosion resistance and adhesion to topcoats, mostly consisting of only organic molecules. Topcoats or paints mainly rely on secondary chemical bonding, i.e., polar interactions such as hydrogen bonds, and van der Waals forces; Conversely, conversion coatings are mostly dependent on primary chemical bonding, or chemisorptions.

1.2.1.2 Corrosion Mechanism under Coatings

Although other factors, such as mechanical stress, chemical attack, internal stress and weathering may cause failures of a coating, the lack of adhesion is always the predominant reason for the failure. When water molecules permeate the organic coating and reach the substrate-coating interface, they cause loss of adhesion, referred to as *wet adhesion*. Leidheiser and Funke (1987) proposed that the loss of adhesion due to water is attributed to chemical disbondment due to chemical interaction of water with covalent, hydrogen or polar bonds, or hydrodynamic disbondment due to water accumulation and osmotic pressures. A corrosion reaction can be initiated by the presence of an aqueous electrolyte with an electrochemical

double layer, a cathodic species (oxygen) and an anodic species (metal). The corrosion reaction proceeds with a constant supply of cathodic species such as water and oxygen (De Wit, 1995).

Figure 1.1 illustrates the formation of a blister under an intact coating due to *cathodic delamination*. After local corrosion initiation, a complex of oxide and hydroxide (represented by the dark color in Figure 1.1a) will be produced and precipitate beneath the polymer, which allows permeation of water but not to oxygen. As a result, cathodic and anodic sites are separated. The anodic area is located under the precipitate while the cathodic reaction is forced to move to the edge of the blister where oxygen may still permeate the coating (Figure 1.1b). The cathodic reaction will increase the pH value at the edge, which causes delamination and further growth of the blister (Figure 1.1c and d).

When a small defect is created in a coating, the metal around the defect will be readily corroded due to the direct exposure to the corrosive media. The corrosion products will block or seal the damaged site for oxygen. Similarly, the separation of anode and cathode will occur and

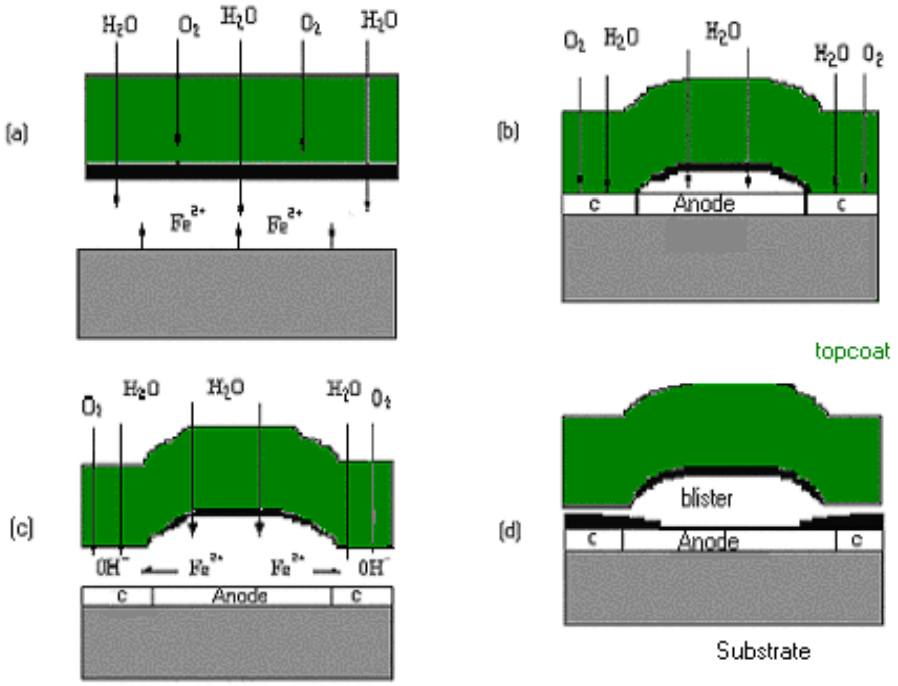

Figure 1.1 Initiation and propagation of a blister due to cathodic delamination under an intact organic coating (De Wit, 1995). (a) initiation of local corrosion due to permeation of water and oxygen; (b) separation of anodic and cathodic sites; (c) propagation of the blister due to the high pH at the edge; (d) formation of a blister under the coating.

corrosion propagation takes place according to the same mechanism.

Anodic delamination may be caused by the dissolution of the substrate metal or its oxides in corrosion-sensitive sites such as an enclosed particle or a scratch under a coating. In contrast to cathodic delamination, the anodic reaction takes place at the blister edge (De Wit, 1995).

Filiform corrosion, a thread-like undermining of the coating, generally occurs in a humid, chloride-containing environments and is common under organic coatings or phosphate coatings on steel, aluminum, and zinc (galvanized steel). Filiform corrosion is a special form of anodic undermining. The basic driving force is a differential aeration cell. Oxygen and water are transferred through the defect; the sites close to this defect are aerated and become the primary cathodic sites; this is the back of the head of the filiform, while the front site of the head is relatively de-aerated and, thus, becomes the primary anodic site, where the metal is oxidized after removal of the oxide by chloride ions. The growth of the filiform continues as the aeration cell is maintained. The corrosion product will remain inside the tail of the filiform (De Wit, 1995).

1.2.1.3 Organic Conversion Coatings

Effectiveness of paints can be significantly increased if metal substrates are pretreated properly. The objective of surface pretreatment is to create proper adhesion of a coating over the substrate. Surface cleaning through abrasive blasting or acid pickling can help remove surface contaminations and create maximum metal reactive sites for better adhesion of the coating (Munger, 1984). The pretreatment coatings (which are also referred to as *conversion coatings*), on the other hand, provide metal substrates with temporary corrosion protection during shipment and storage. They also strengthen the adhesion of paints by providing anchor points for topcoats. The common conversion coatings for metals are inorganic phosphates and chromates. A steel plate can be sprayed or immersed in a dilute solution of phosphoric acid containing zinc, iron or manganese phosphates. Chemically, a zinc-based phosphating solution produces phosphophyllite ($Zn_2Fe(PO_4)_2.4H_2O$) with small amounts of hopeite ($Zn_3(PO_4)_2.4H_2O$). A phosphate layer provides a secondary barrier to corrosion and increases wear resistance, but it is used primarily as a base for paints on such products as automobile bodies and refrigerator cabinets. The phosphate coating improves paint adhesion, retards the spread of corrosion, and provides a dielectric coating to insulate anodic and cathodic sites on steel surface. The phosphate coatings are crystalline and porous; therefore, the pores are usually sealed by oil or chromate spray.

Chromate coating is formed on steel by contacting a solution of chromic acid and sulfuric acid containing activators such as sulfate, formate, chloride, etc. It contains both trivalent and hexavalent chromium ($Cr_2O_3.CrO_3.nH_2O$). The hexavalent chromium (Cr^{6+}) slowly leaches from the film in the presence of atmospheric moisture and adsorbs on the exposed area of the substrate. The Cr^{6+} ions act as an oxidizing agents for the exposed area of the substrate and provide passivation. This phenomenon is known as *self-healing*. Usually, significant corrosion does not occur until all of the hexavalent chromium has been leached out. There is an optimum Cr^{6+}/Cr^{3+} ratio in the film. An excessive amounts of hexavalent chromium do not show beneficial effects. Chromating is used on galvanized steel to prevent the formation of white rusting during transportation and storage.

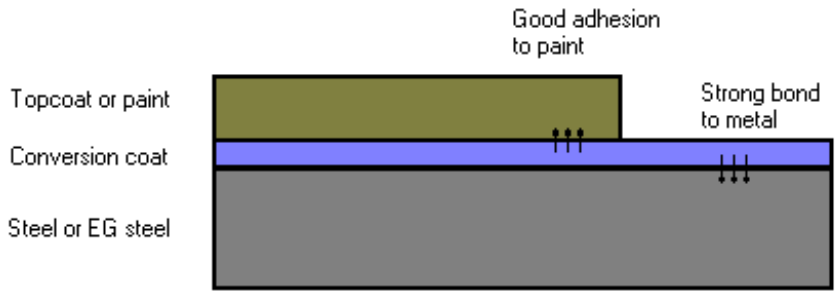

Figure 1.2 Schematic illustration of an organic conversion coating on cold-rolled steel (CRS) sheet

Because of the toxicity of chromium, the chromating process is subjected to stringent governmental regulations. Therefore, organic conversion coatings have been widely pursued as an alternative to the chromating process in the steel industries worldwide. Figure 1.2 presents a schematic description of organic conversion coatings on cold-rolled steel sheet (CRS). This conversion coating has to possess a desirable anti-corrosion property, good paintability and acceptable machinability.

In order to avoid rusting during shipment and storage, the organic conversion coating on steel sheet is usually required to withstand 72-150 hours of salt spray in a salt spray chamber designated by ASTM standard B 117-97 (Kubota, 2000). Corrosion inhibition produced by the coating depends on the composition, structure and thickness of the coating, which affect oxygen

and water permeability, as well as chemical bonds of the metal/organic coating interface. Generally, a close-packed, thick and hydrophobic film formed on the metal substrate is critical to inhibit corrosion by retarding the transport of charged species (ions) and uncharged species (water, oxygen), which affect the corrosion behavior in a paint/metal systems (Miskovic-Stankovic, 1997). A robust organic film will have less porosity and a diffusion path to the external corrosive media. However, the need for corrosion inhibition has to be compatible with the need for spot welding and electrical grounding. A thick insulating film can increase corrosion resistance, but it may deteriorate the steel's grounding properties and weldability. To obtain good grounding and weldability, the thickness of the conversion coating should be less than 1 to 2 μm. It still remains a challenge to achieve good corrosion protection with thin films without the use of chromate (Kubota, 2000).

In addition to corrosion resistance and grounding properties, paint adhesion (or *paintability*) is another consideration of conversion coatings. It is universally accepted that adhesion is comprised of three components: primary chemical bonding (ionic or covalent bond), secondary (polar) bonding, and mechanical bonding. For topcoats or paint, primary chemical bonding to the substrate is relatively rare; they mainly rely on secondary chemical bonding, i.e., polar interactions such as hydrogen bonds and van der Waals forces (Weldon, 2001). Conversely, conversion coatings are mostly dependent on primary chemical bonding, or chemisorptions. Obviously, *wetting* is a major factor in adhesion. In other words, adhesion cannot occur if the paint or coating does not spread spontaneously over the substrate surface so that there is intermolecular contact between the solid and the liquid (Wicks, 1994). Figure 1.3 shows a

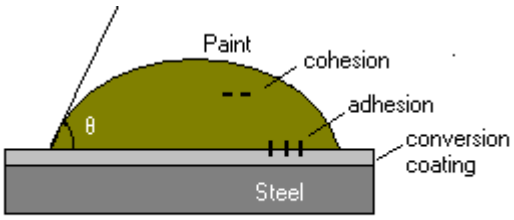

Figure 1.3 Schematic of a paint drop applied onto a coated-steel surface. θ is the contact angle at equilibrium state.

schematic drawing of a drop of paint with intermediate surface tension on a coated steel surface.

The ease of spreading of a liquid paint on a solid surface depends mainly on the paint/substrate interaction, represented by the work of adhesion (W_a), which is mostly dominated by the surface free energy (also called the surface tension) of both the paint and the solid if no chemical reaction is involved. The work of adhesion (W_a) between the solid and the liquid can be expressed by the Duper Equation:

$$W_a = -\Delta G = \gamma_L + \gamma_S - \gamma_{SL} \quad [1.1]$$

where, γ_L, γ_S and γ_{SL} are the surface tensions of the liquid-air, solid-air, and solid-liquid interface, respectively. ΔG is the Gibbs free energy of adhesion.

The cohesion work of the paint: $Wc = 2\,\gamma_L$ [1.2]

Young's equation: $\cos(\theta) = \dfrac{\gamma_S - \gamma_L}{\gamma_{SL}}$ [1.3]

The combination of Equations [1.1] and [1.3] gives the solid-liquid work of adhesion, as expressed by the Young-Duper equation:

$$W_a = \gamma_L (\cos\theta + 1) \quad [1.4]$$

The spread coefficient (S_{LS}) is defined by Harkins equation:

$$\begin{aligned} S_{LS} &= W_a - W_c \\ &= \gamma_S - (\gamma_L - \gamma_{SL}) \\ &= \gamma_L (\cos\theta - 1) \end{aligned} \quad [1.5]$$

Therefore, spreading spontaneously occurs if the spreading coefficient has positive values, In other words, the work of adhesion must be larger than that of cohesion. Otherwise, the liquid cannot wet the solid surface, but will bead up with a very high contact angle. Apparently, spreading or wetting is favorable if γ_S is greater than γ_L. The factors that influence the surface tension of paints are temperature, solvents, additives and resin type. The surface tension of the substrate is dictated by its chemical composition and its cleanliness (Weldon, 2001).

A good conversion coating should also possess an anti-fingerprint properties to prevent the coating surface from contamination during shipment and forming. Otherwise, the area of a steel

sheet where fingerprints are located may become nuclei of corrosion due to the moisture and salt secreted by humans. Fingerprints also present an ugly appearance on steel sheets. A hydrophobic surface, usually but not necessarily, renders good anti-fingerprintability.

1.2.2 Carboxylates as Corrosion Inhibitors

1.2.2.1 General Information

The use of inhibitors is one of the most universal and economical measures used to combat corrosion of metals. When present in small quantities in an aggressive medium, they retard corrosion by bringing about changes in the surface condition of a metal. Traditional inhibitors include either inorganic compounds having oxidizing properties (chromates, nitrites) or those capable of forming sparsely soluble salt films on the metal surface. Organic compounds of various chemical compositions can prevent the local depassivation of metals (i.e., pitting) as a result of adsorption. Of the organic inhibitors, carboxylic acids, also referred to as fatty acids, with the general formula, RCOOH, have received much attention. They may either be added to the corrosive media as inhibitors, or form a monolayer on metal substrates, acting as protective films (Ulman, 1991; Kuznetsov, 1996).

1.2.2.2 Formation and Structure of Carboxylate Film

Spontaneous adsorption of long chain n-alkanoic acids on aluminum oxide, silver, etc., has been studied extensively (Allara and Nuzzo, 1985a and b; Ogawa, 1985; Schlotter, 1986). Film thicknesses of C14, C16, C18, C20 and C22 carboxylic acid on aluminum oxide substrates showed agreement with the all-trans extended molecular length (Allara and Nuzzo, 1985a, b). Chen and Frank (1989) found that the time required to reach maximum hydrophobicity increased with decreasing concentration of the stearic acid monolayers on both aluminum and glass substrates. It requires much higher concentrations to produce good monolayers on glass (10^{-2} *M*) than on Al_2O_3 (10^{-4} *M*). This concentration dependence is in agreement with the expected affinity.

Chapman and Tabor (1957) pioneered the study of SAMs of fatty acids ($C_nH_{2n+1}COOH$, n=1~45) by electron diffraction. They found the area per molecules (on silver and palladium) was 21.3 $Å^2$, quite different from that in bulk fatty acids and paraffin crystals (18.8 $Å^2$) and from that in a water-air interface monolayers(20.4 $Å^2$). Grazing incidence *X*-ray diffraction of

docosanoic acid ($CH_3(CH_2)_{20}COOH$) monolayer on AgO revealed a p(2×2) overlayer structure with a lattice spacing 5.78 Å and alkyl chains tilted by 26.7° from the surface normal (Smart, 1993). Huang and Tao (1986) studied SAMs of long-chain diacetylene amphiphiles (R_1-C≡C-C≡C-R_2). The diacetylene units may introduce a stream of defects into this assembly and are not beneficial to the ordering if they are located far from the carboxylic head group. Zhou, et al. (2000) studied the UV polymerization of *10,12*-pentacosadiyonoic acid ($CH_3(CH_2)_{11}$-C≡C-C≡C-$(CH_2)_8COOH$) monolayers at varying surface pressures and temperatures and confirmed the molecular packing in the monolayer.

1.2.2.3 Corrosion Inhibitive Performance

Carboxylates have long been used as corrosion inhibitors for metals, especially for aluminum. According to Kuznetsov (1996), an increase in the length of carbon chain in the anion ($RCOO^-$) has a beneficial effect on inhibition efficiency due to the increase of hydrophobicity. The presence of a double bond in the molecules of carboxylic acid usually increases its polarizability and thereby its inhibiting effectiveness. Sodium *6*-undecylenate ($CH_3(CH_2)_3CH=CH(CH_2)_4$-COONa) is one of the most effective olefinic carboxylates, although it is not a particularly good surfactant (HLB=21.3). In the case of aluminum protection, sodium oleate ($CH_3(CH_2)_7CH=CH$-$(CH_2)_7COONa$) is an effective inhibitor in neutral media, while sodium stearate ($CH_3(CH_2)_{16}$-COONa) is a weak inhibitor despite its surface activity (Table 1.1). As for cyclic compounds, the effectiveness is to a large extent determined by their hydrophobicity. *11*-phenylundecanoate ($C_6H_5(CH_2)_{10}COONa$) has a high passivating ability on various metals. In practice, mixtures of several inhibitors are used to enhance the protective action by the synergistic effect.

The inhibiting effect ΔE shown in Table 1.1 is defined as follows:

$$\Delta E = E_{pit}^{inh} - E_{pit}^{backgroud} \qquad [1.6]$$

where, E_{pit} is the pitting potential at breakdown of the passive state. The addition of anion inhibitors usually drives E_{pit} to more positive values and hinders depassivation, even completely prevents it, at least up to the potential of oxygen evolution (E_{O2}).

Table 1.1 Surface protective properties of higher olefinic carboxylates for aluminum in 0.01 *M* buffer solution (pH=8.1) of NaCl, $E_{pit}^{backgroud} = -0.33V$ (Kuznetsov, 1996)

Inhibitors	CMC $M, \times 10^5$	ΔE (V) 0.001 *M*	0.005 *M*	0.01 *M*
Sodium Sterate	6	0.025	0.065	---
Sodium oleate	15	0.09	0.32	0.47
Sodium linoleate	75	0.26	0.53	0.73
Sodium linolenate	80	0.32	0.62	0.83
Sodium ricinoleate	40	0.09	0.36	0.66

Bereket and Yurt (2001) found that the addition of 10^{-2} *M* hydroxyl-carboxylic acids (R(OH)CHCOOH) or amino acids ($R(NH_2)CHCOOH$) to NaCl solutions causes shifting of E_{pit} values to the noble direction. Amino acids are more effective in acidic solution while hydroxyl carboxylic acids are favorable in neutral or basic solution.

Schulman and Bouman (1997) used long-chain carboxylic acids, preferably isostearic acid, as organic seals for anodized aluminum. Salt spray tests showed that its corrosion resistance was superior to that obtained with chromates. The organic seals also exhibited the healing capacity of chromates, i.e., they can form a hydrophobic surface with reactive ingredients to repair damage. The authors suggested that the same technique could be used for steel, if it is coated with aluminum, anodized, and sealed with fatty acids.

Hefter, et al. (1997) used straight chain carboxylates as organic corrosion inhibitors for steel, copper and aluminum. When they used dicarboxylates, the longer carbon chain gave better corrosion inhibition. For monocarboxylates, there was an optimum intermediate chain length for effective corrosion inhibition. The dramatic variations in inhibitor efficiencies probably resulted from competing reactions, such as adsorption and complexation at the metal (hydroxide) surface, solubility, and micelle formation. Similarly, electrochemical measurements (R_p, i_{corr}) conducted by Rocca, et al. (2001) revealed that the inhibiting efficiency of sodium monocarboxylates ($CH_3(CH_2)_{2n-1}COONa$, n=7~11) in the aqueous corrosion of lead was dependent on the carbon chain length and the concentration.

Park, et al. (1999) used *10*-undecenoic acid (UA, $CH_2=CH(CH_2)_8COOH$) to synthesize a new class of polymer films on a platinum electrode by plasma polymerization techniques. The crosslinking density of the polymer film can be modulated by step-wise variation of the plasma power. The film thickness increased almost linearly with the increase in the plasma duration, and the deposition rate of the film was 13 nm/min.

Fousse (1999) patented a surface treatment process for metal sheets such as bare steel, and zinc-, chromate-, tin-plated steel. A thin organic film was produced with a chemical containing an apolar alkyl chain on one end and a polar radical on the another end, for instance, oleic acid, or palmitic acid. The sheet with the organic film is then heated to a suitable temperature for a suitable time (e.g., 1 second to 10 minutes at >120 °C for oleate) to enhance its reaction with the metal surface and to make it partly crosslink through physical entanglement.

Aromatic carboxylic acids (e.g., ω-benzoyl alkanoic acid, $R\text{-}C_6H_4\text{-}CO(CH_2)_nCOOH$) are found to form a passive film on iron surfaces, capable of inhibiting the anodic partial reaction. The stability of this passive film under anodic polarization conditions decreases in the order $ClO_4^->Cl^->SO_4^{2-}$ for different electrolytes (Agarwal and Landolt, 1998). The influence of the nature and concentration of electrolyte anions may be attributed to the competitive adsorption mechanism between the inhibitor anions and other electrolyte anions, e.g., SO_4^{2-} and Cl^- (Olsson, 2000).

1.2.3 Silanes as Coupling Agents

1.2.3.1 Chemistry of Silanes

Various forms of silanes are used as coupling agents in fiberglass-reinforced resins and organic coatings. The commonly used silane coupling agents are organosilicon monomers of the general formula: $Y(CH_2)_nSiX_3$, where n=0~3, X is an easily hydrolysable group (e.g., Cl, CH_3O, or C_2H_5O), Y is a functional group designed to react with or be compatible with a given resin. Non-functional silanes or silane crosslinkers have the structure $X_3Si(CH_2)_mSiX_3$ where one example is m=2.

The functional group of silane is formed mostly through the addition of silicon hydrides to substituted olefin and acetylenes, as expressed with the following reaction (Plueddemann, 1991):

$$X_3SiH + CH_2=CHR' \rightarrow X_3SiCH_2CH_2R' \qquad [1.7]$$

Table 1.2 Selected commercial silane coupling agents used in protective coatings

Organofunctional group	Chemical structure
Vinyl	$CH_2=CHSi(OCH_3)_3$
	$CH_2=CHSi(O_2CCH_3)_3$
Chloropropyl	$Cl(CH_2)_3Si(OCH_3)_3$
Epoxy	$CH_2(\text{-O-})CHCH_2O(CH_2)_3Si(OCH_3)_3$
Methacrylate	$CH2=C(CH_3)COO(CH_2)_3Si(OCH_3)_3$
Primary amine	$H_2N(CH_2)_3Si(OC_2H_5)_3$
Diamine	$H_2NCH_2CH_2NH(CH_2)_3Si(OCH_3)_3$
Mercapto	$HS(CH_2)_3Si(OCH_3)_3$
Cationic styryl	$CH_2=CH(C_6H_4)CH_2NHCH_2CH_2NH(CH_2)_3Si(OCH)_3HCl$
Cycloaliphatic epoxide	$CH_2(\text{-O-})CHCH_2CH_2Si(OCH_3)_3$

Where the CH_2CH_2R' is the $Y(CH_2)_n$ group. This reaction can happen in both liquid and gas phase, and can be catalyzed by peroxides, tertiary bases, or platinum salts. Examples of Y groups are -Cl, $-NH_2$, -SH, $-CH=CH_2$, -N=C=O or $-OCOC(CH_3)=CH_2$, etc. Alkoxysilanes are often prepared by alkoxylation of chlorosilanes. Examples of the X group are $-OCH_3$, $-OC_2H_5$, and $-OCOCH_3$, etc. Table 1.2 lists some of the commercial silane coupling agents.

1.2.3.2 Deposition of Silanes on Metal Substrates

Silane-coupling agents are often applied from dilute water solutions or organic solutions containing water. Silanes can function as an efficient chemical bridge between polymers and inorganic surface only when the alkoxysilane (Si-OR) groups are hydrolyzed to silanols (Si-OH) (Pu, 1997; Leyden, 1991). The hydrolysis reaction can be expressed as follows:

$$Y(CH_2)_nSiX_3 + 3H_2O \Leftrightarrow Y(CH_2)_nSi(OH)_3 + HX \qquad [1.8]$$

Silanols produced by hydrolysis will further condense to oligomeric or polymeric siloxanes ((Si-O-Si) (Ishida, 1983; Walker, 1987; Comyn, 1986). The condensation reaction, as represented in equation 1.9, is relatively slow in comparison with the fast hydrolysis reaction,

depending on the organofunctionality, water content, temperature, and pH of the solution (Shih and Koenig, 1975; Tesoro and Wu, 1991).

$$\underset{\text{(dimer)}}{\text{-SiOH}} + \text{HOSi-} \Leftrightarrow \underset{\text{(oligomer)}}{\text{-Si-O-Si-}} + H_2O \qquad [1.9]$$

The trihydroxy silanes formed may be crosslinked *via* siloxane bonds and become a polymeric species, which in turn adsorbs on a substrate *via* H-bonding and then eventually forms a stable covalent bond with the substrate as shown in Figure 1.4. It is possible, however, that hydroxyl silanes adsorb individually on a surface and then undergo crosslinking polymerization. This is a widely postulated binding mechanism between silane and inorganic substrate (van Ooij, 1991 and 1993c; Sabata, 1993; Petrunin, 1996; Yuan, 1997; Stevens, 1999; Kurth, 1995; Quinton, 1997; Bell, 1991; Lin, 1991).

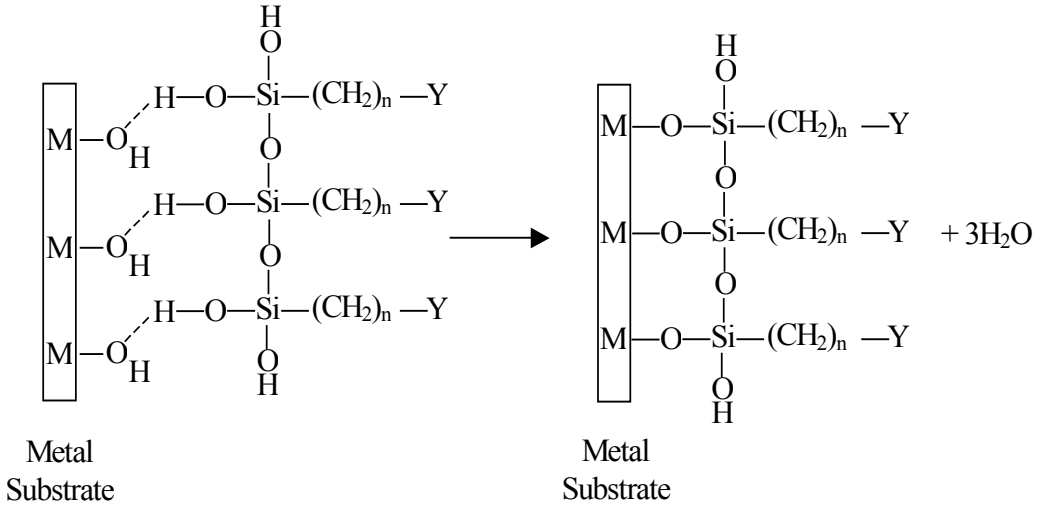

Figure 1.4 Adsorption of a hydrated organofunctional silane on the surface of a hydroxylated metallic substrate. Initial adsorption mechanism involves H-bonding, followed by condensation reaction to form M-O-Si bonds.

Figure 1.5 is a schematic representation of how the silanes adsorbed on a metal substrate work as coupling agents. A resin interacts with the functional groups (Y) of the silane molecules, providing a bonding mechanism between the organic topcoat and the inorganic substrate. For a resin whose functional groups are acidic, Y is selected to be basic or *vice versa*.

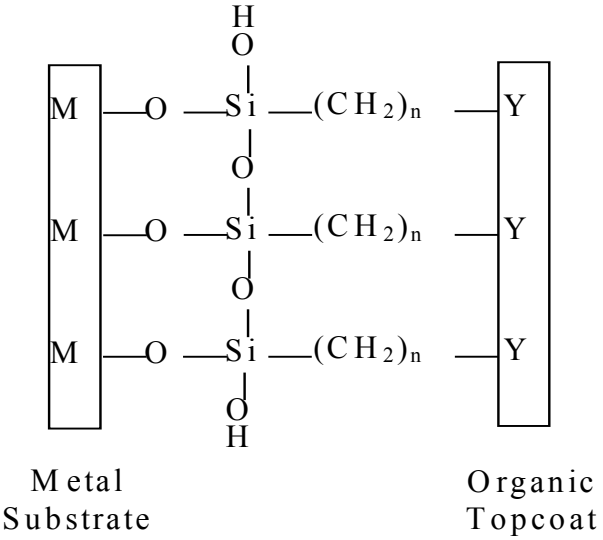

Figure 1.5 Schematic representation of a hydrated silane working as a coupling agent. The molecule has affinity to both the inorganic substrate and an organic topcoat.

Thus, the interaction between Y and organic resin is mainly governed by the acid-base interaction mechanism.

Thus, the driving force for the adsorption of silanes on an inorganic substrate is covalent bonding (M-O-Si) with the substrate and siloxane bonding (Si-O-Si) between neighboring molecules. Both bonding mechanisms contribute to the large negative free energy of adsorption, which is probably the reason that silanes form robust surface coatings.

A two-step silane treatment has been developed by Child, et al.(1999), as illustrated in Figure 1.6. A non-organofunctional silane (BTSE) is deposited on the metal substrate. Because BTSE is a stronger acid, it reacts more readily with the weakly hydroxyl groups on the metal oxide surface and forms covalent, hydrolysis-resistant bonds. But the BTSE film does not react with many polymers, because it has no functional group. However, many of its silanol groups can react with other silanol groups. Therefore, a second organofunctional silane (e.g., VS) can be deposited on the top of the BTSE film before it is completely crosslinked. The resulting multilayer silane film is more stable in water or salt solutions. It is also more compatible to topcoats due to the high degree of organofunctionality in the surface layer.

A hydrolyzed silane can be contacted directly with an inorganic surface by dipping, spraying, and brushing. Generally, a clean and stable hydroxylated oxide layer is desired for silane

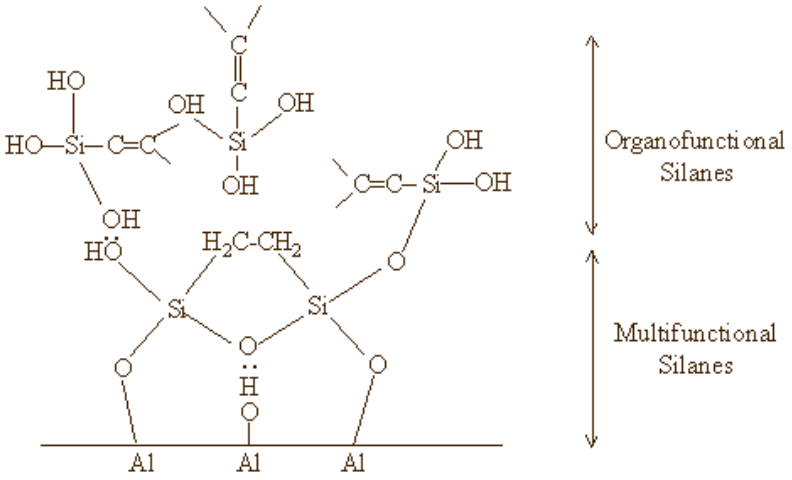

Figure 1.6 Schematic of a BTSE/VS bilayer formed on aluminum (Child, 1999)

coupling agents. The concentration and pH of silane solutions are the most important parameters affecting the hydrolysis and condensation reaction, and, ultimately, the reactivity and stability of silanes.

1.2.3.3 Corrosion and the Adhesion Performance

Van Ooij, et al. of University of Cincinnati developed methods of using various silanes for corrosion inhibition of steel and other metals. They have obtained four different groups of U.S. Patents. The first group of U.S. patents, which includes No. 5,108,793 (1992) and No. 5,200,275 (1993a), disclosed methods of rinsing steel sheet for about 30 seconds in an alkaline solution containing 0.05 *M* sodium silicate (water glass) and 0.005 *M* $Ba(NO_3)_2$, $Ca(NO_3)_2$, or $Sr(NO_3)_2$ at elevated temperature (>45 ^oC) and pH (<10). The steel sheet is then dried to form a relatively insoluble silicate coating. The silicate-coated surface is then rinsed with a solution containing 0.5~5.0% silane by volume. γ-APS shown in Table 1.3 is one of the silane-coupling agents disclosed in the first group of patents.

In U.S. Patent No. 5,322,713, van Ooij (1994b) disclosed a method of coating steel with aluminate rather than silicate before silanation. The aluminate coating is carried out in an alkaline solution containing $NaAl(OH)_4$, $KAl(OH)_4$ and $LiAl(OH)_4$ in the presence of a metal salt selected from calcium, strontium, and barium nitrates.

The second group of U.S. patents developed by van Ooij includes No. 5,455,080 (1995b), No. 5,498,481 (1996a) and No. 5,539,031 (1996b). These patents disclosed a method of firstly

coating steel with an inorganic layer such as silicate and then coating it with a powder consisting of a thermosetting resin (epoxy, polyester, epoxy-polyester, acrylic, acrylic-urethane or fluovinyl), a solid (-325 mesh), and a silane-coupling agent. The steel plate is then cured at a temperature (100~250^{o}C) above the melting point of the thermosetting polymer. While the steel is maintained at the curing temperature, the silane-coupling agents diffuse to the substrate where the crosslinked layer is coupled to the inorganic layer by organosilane.

The third group of U.S. patents (No. 5,292,549, No. 5,433,976, No. 5,750,197) developed by van Ooij, et al. (1994a, 1995a and 1998a) disclosed a method of using both a crosslinking silane and a functionalized silane. The crosslinking silanes (or multifunctional silanes) are those that have silane groups at both ends of an alkyl chain. An example is *1,2-bis*(triethoxysilyl) ethane (BTSE) shown in Table 1.3. Crosslinking silanes bond strongly to the inorganic substrate, while functionalized silanes adsorb on the top of the crosslinking silanes adsorbed on the surface. In the U.S. Patent No. 5,433,976 issued to van Ooij and Sabata (1995a), steel sheet is coated with silicate or aluminate in the same manner as described in the first group of patents prior to silanation.

In the U.S. Patent No. 5,292,549 (van Ooij, 1994a), a steel sheet is first rinsed with a solution containing both organofunctional silane (0.5~2.0% by volume) and crosslinking silane (0.1~1.0% by volume), and then cured at 200 ^{o}C. This method allows the metal sheet to be coated directly by the silane coupling agents without silicate or aluminate coatings. One drawback of this method is that the organofunctional silanes do not bond well to the metal surface, and, thus, the coating is easily rinsed off.

In the U.S. Patent No. 5,750,197 (van Ooij, 1998a), the metal sheet is coated first with a crosslinking agent (or multifunctional silane) alone without an organofunctional silane, which apparently strengthens the bonding. If the metal is to be painted or coated with another polymer, organofunctional silane is applied as a second coat on the top of the first coat of multifunctional silane. The best multifunctional silane reported by van Ooij is BTSE. The organofunctional silanes that were used in conjunction with multifunctional silanes include γ-APS, γ-UPS, SAAPS, which are listed in Table 1.3. In the US Patent No.6,261,638 B1 (van Ooij, 2001), a multi-functional silane having at least two trisubstituted silyl groups such as alkoxy and acetoxy was used as the first coating for metal substrates to prevent corrosion.

The U.S. Patent No. 5,759,629 represents the fourth group of patents of van Ooij, et al. (1998b). In this method, the metal sheet is treated with a solution containing at least one vinyl silane. The vinyl silanes disclosed in this patent include organofunctional silanes of a general formula: $Y(CH_2)_nSiX_3$, where Y is $-CH=CH_2$, and *N*-(*2-9*-vinylvenzylamino)-ethyl-*3*-amino-propyltrimethoxysilane. In the former, the value of n ranges from 0 to 10. For longer chain silanes, it is necessary to use short-chain alcohols rather than water as solvents. The vinyl silane

Table 1.3 Silane coupling agents (van Ooij and Child, 1998c)

Compound name	Acronym	Formula	Metals treated
γ-Aminopropyl silane	*γ*-APS	$H_2N(CH_2)_3Si(OC_2H_5)_3$	Iron, aluminum
γ-Ureidopropyl silane	*γ*-UPS	$H_2NCONH(CH_2)_3Si(OC_2H_5)_3$	Zinc
1,2-bis(triethoxysilyl)ethane	BTSE	$(C_2H_5O)_3Si(CH_2)_2Si(OC_2H_5)_3$	Iron, aluminum
Styrylaminoethylamino-propyl-trimethoxysilane	SAAPS	$H_2C=CH-C_6H_4CH_2NHCH_2NH-(CH_2)_3-Si(OCH_3)_3$	Galvalume
Vinyl silane	VS	$H_2C=CHSi(OCH_3)_3$	Zinc

coating not only provides a surprisingly high degree of paint adhesion, but also prevents delamination and underpaint corrosion. Vinyl silanes are good for galvanized steel but not for bare steel, as indicated in Table 1.3.

The U.S. Patents No. 5,326,595 (Shuford, 1994), No. 5,326,594 and No. 5,478,655 (Sabata, 1994, 1995) and No. 5,700,523 (Perole, 1997) showed methods of coating metal sheets with silicate and aluminate before applying aqueous solutions of organofunctional silanes. These methods are similar to the second group of van Ooij's U.S. Patents described above.

In a series of U.S. Patents authored by Blohowiak (1998a, b and c; 1999), the Boeing Company disclosed a method of producing strong adhesive bonds between aluminum and resin with silane coupling agents. This method consists of contacting metal sheet with an aqueous sol containing zirconium, organosilane, organic acid catalyst, and alkoxyzirconium stabilizer.

The US patents No. 4,618,688 and No. 4,645,846 authored by DePasquale, et al. (1986, 1987) disclosed a novel class of alkoxy silanes as corrosion preventive coatings. These

compounds contain an amine or an amine group in a linear or cyclic structure. Sulfur and/or a carbonyl or thiocarbonyl group may also be present.

A series of US Patents authored by Castellucci (1993a, 1993b, 1994) showed a process for producing a novel corrosion-resistant conversion coating on a metallic surface having exceptional durability. The silane polymer coating which was applied to the metal surface was fabricated by anhydrously reacting an epoxy trialkoxy silane with a primary aminotrialkoxy silane in a stoichiometric molar ratio.

In US patent No. 5,221,371, No. 5,356,492, No. 5,399,210 and No. 5,419,790, Miller (1993, 1994, 1995a, b) disclosed a three-step process to produce a non-toxic corrosion resistant conversion coating for aluminum and its alloys. The metal is pretreated with an acidic solution containing K_2MnO_4 or H_2O_2, cereous chloride, alone or in combination with strontium chloride. The corrosion resistance is improved by a subsequent treatment in an alkaline solution containing molybdate, nitrite and metasilicate ions, and is further improved by treating the coated surface with an alcoholic solution containing glycidoxy (epoxy) polyfunctional methoxy silane, alone or in combination with phenytrimethoxysilane.

Page and Plueddemann (1991) reported several techniques for improving the performance of silane coupling agents: (1) blend hydrophobic silanes with hydrophilic ones to give greater hydrophobic character; (2) use more thermally stable silanes such as phenyltrimethoxysilane to give increased thermal stability.

Silanes are good coupling agents between inorganic substrate and the organic coating. They have great potential for use in corrosion prevention technically. However, cost is a disadvantage for large-scale applications.

1.2.4 Self-Assembled Monolayers (SAMs) of Thiols

1.2.4.1 General Information

A self-assembled monolayer (SAM) is a molecular assembly formed on a substrate spontaneously by adsorption of an active surfactant and chain-chain reorganization. This monolayer features a high degree of orientation, molecular order and packing. Figure 1.7 shows a schematic model of a SAM on a solid substrate. It consists of active head groups chemisorbed on the substrate, chains or backbones bound together by van der Waals forces, and tail groups at the air-monolayer interface. A typical example is the alkylsiloxane, fatty acids and alkanethiol monolayers. All these systems have already been reviewed in great detail (Ulman, 1991, 1996a;

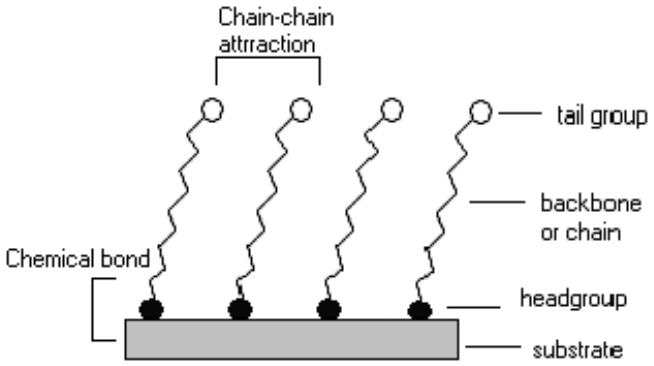

Figure 1.7 Schematic model of self-assembled monolayers (SAMs) on an ideal metal substrate

Tredgold, 1994; Finklea, 2000; Schreiber, 2000). This section gives a brief review of the application of thiol-type SAMs in corrosion prevention.

Thiols (R-SH, where R denotes the rest of the molecule) on gold and silane on SiO_2 are identified as two model systems. Thiol (R-SH) can form an excellent SAM on Au(111) substrates. The head groups adsorb onto the gold strongly, and preferentially. The molecules reorganize themselves through the chain-chain interaction, creating a dense monolayer with tail groups pointing outwards from the surface.

By using thiol molecules with different tail groups, the functionality of the resulting chemical surface can be tailored within wide limits. Alternatively, it is also possible to chemically modify the tail groups by performing reactions even after assembly of the SAM. Due to its unique surface properties and the tunability of surface properties *via* modification of molecular structure and functions, SAMs can be potentially applied in many areas such as wetting, lubrication, adhesion, corrosion, biocompatibility, catalysis, chemical sensing, electronic device, and nanoscale lithography (Ulman, 1991; Schreiber, 2000).

1.2.4.2 Synthesis of Alkanethiols

According to Laibinis (1998), the commercially available thiols are primarily limited to unsubstituted alkanethiols ($CH_3(CH_2)_nSH$, n=0~9,11,13,15,17) that produce low-energy methyl surface, and short-chained substituted alkanethiols ($HS(CH_2)_nX$, n=1,2 for X=CO_2H, CO_2CH_3, $CO_2CH_2CH_3$ and n=2 for X=NH_2 and OH). The synthetic methods of alkanethiols introduced

below are quoted from Laibinis's paper (1998), from which one may find the original sources for more details.

Long-chained alkanethiols ($CH_3(CH_2)_{2n-1}SH$, n=5~9) may be synthesized through the conversion of alcohols to thiol either directly [eq. 1.10a], or from terminal olefins [eq. 1.10b] or converting alcohols into alkyl bromides [eq. 1.11a], and subsequently displacing bromide with NaSH [eq. 1.11b].

$$CH_3(CH_2)_{2n-1}OH + H_2S \rightarrow CH_3(CH_2)_{2n-1}SH \quad [1.10a]$$

$$CH_3(CH_2)_{2n-3}CH{=}CH_2 + H_2S \rightarrow CH_3(CH_2)_{2n-1}SH \quad [1.10b]$$

$$CH_3(CH_2)_{2n-1}OH + HBr \rightarrow CH_3(CH_2)_{2n-1}Br \quad [1.11a]$$

$$RBr + NaSH \rightarrow xRSH + yRSR + NaBr \quad [1.11b]$$

However, the first two reactions are not preferred practically because of the harsh conditions and the toxicity of H_2S. The second synthesis route leads to the formation of both thiols and sulfides, resulting in reduced yield and difficulty in separation.

The common methods for replacing a halide with a thiol are two-step procedures that use thiourea, and are followed by a solvolysis step under acidic or basic conditions [eq.1.11].

$$RBr + H_2NCSNH_2 \rightarrow RSC(NH_2)_2Br \quad [1.12a]$$

$$RSC(NH_2)_2Br + (\text{amine or acid})/R'OH \rightarrow RSH + H_2NCONH_2 \quad [1.12b]$$

1.2.4.3 Formation of Thiol Films

Sulfur compounds have a strong affinity for a transition metal surfaces. The specific affinity between sulfur and metal makes the organosulfur surfactants the most studied molecules that form SAMs on metal substrates. These include, among others, alkanethiol (R-SH), dialkyl disulfide (R-S-S-R), dialkyl sulfide (R-S-R), alkyl xanthate ($R\text{-}O\text{-}CSS^-$) (Gothelf, 2000), and dialkyl thiocarbamate (R_2NCSS^-). Thiol on Au(111) has been extensively studied as a model

system because of the relative inertness and well defined microcrystalline surface of gold, making it easy to clean and prepare. Other substrates used for forming thiol-type SAMs include silver, platinum, copper, iron, nickel, liquid mercury, and semiconductor surfaces (GaAs, InP, etc.) (Ulman, 1991, 1996a; Finklea, 2000; Schreiber, 2000).

Because *n*-alkanethiols are fully saturated and fairly simple compounds, their small terminal groups facilitate the formation of densely packed, often crystalline, SAMs on gold, they are commonly used as an archetypal model of thiols on gold, (Laibinis, 1998; Schreiber, 2000). We will focus on this model system to describe the formation, structure and surface properties of SAMs.

(1) Process of adsorption and Self-assembly

In situ AFM monitoring shows that the self-assembly process may be broken down into three steps, as illustrated in Figure 1.8, i.e., mobile phase, lying-down phase and standing-up phase (Camillone, 1996; Liu, 1998). During the initial adsorption, the height of spikes is 4.2 Å (equal to the diameter of hydrocarbon chains) and all spikes are parallel to the scanning direction, indicating rolling or sliding molecules. Higher surface coverage results in less mobility for these lying-down molecules and causes the spikes to disappear completely. As the adsorption

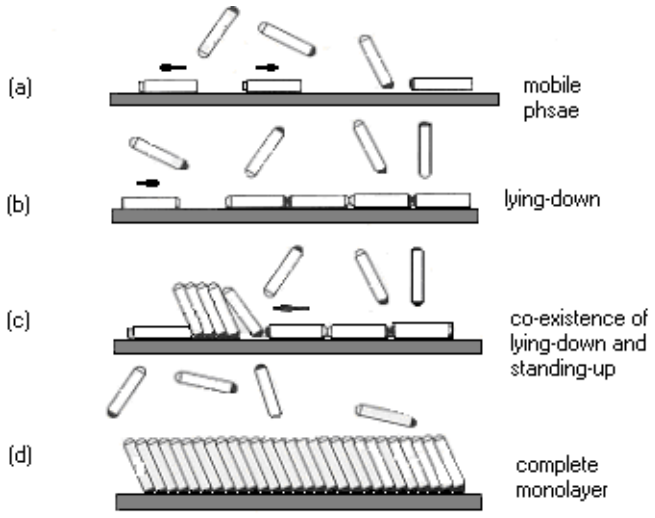

Figure 1.8 Schematic diagram of the proposed self-assembly mechanism of ODT ($CH_3(CH_2)_{17}SH$ on gold (Liu, et al., 1998). (a) mobile phase; (b) lying-down phase; (c) coexistence of lying-down and standing-up phase; (d) complete monolayer.

proceeds, the coverage continues to increase and elevated islands of 20~100 Å in lateral dimension appear. The height between the islands and the lying-down domains is 15±2 Å, which suggests that the elevated islands are close-packed *1*-octadecanethiol (ODT) molecules with a tilt angle of ~27^{o}.

Long-term effects in the ordering process were recently investigated with Sum Frequency Generation (SFG) (Himmelhaus, 2000). Three steps of the self-assembly process were also identified, each with its own time scale and characteristic vibrational spectra. The faster step is related to the chemisorption of the headgroups within ~5 minutes. The second step is 3~4 times slower than the first step, involving the straightening of the hydrocarbon chains. The third and final step is related to the reorientation of the terminal group, 35~70 times slower than the second step. This result is in consistent with *in situ* AFM observation discussed above.

(2) Thermodynamics of SAM formation

According to Ulman (1991), the adsorption mechanism of alkanethiol onto gold (0) is not yet completely understood. The formation of RS-Au^{+} requires the loss of the SH hydrogen, but it is not clear yet whether this proton is lost as H_2, as expressed in equation [1.13], either via the reductive elimination reaction of the gold (I) hydride (RS-Au^{2+}-H^{-}), or by another unknown reaction,

$$RS\text{-}H + Au^{0}_{n} \Rightarrow RS^{-}\text{-}Au^{+} + \tfrac{1}{2}\, H_2 + Au^{0}_{n-1} \qquad [1.13]$$

or as H_2O, either by the reaction of either the gold (II) hydride or another unknown species with traces of oxidant,

$$RS\text{-}H + Au^{0}_{n} + \text{oxidant} \Rightarrow RS\text{-}Au^{+} + \tfrac{1}{2}\, H_2O + Au^{0}_{n-1} \qquad [1.14]$$

Karpovich, et al. (1998) proposed that the initial adsorption reaction can proceed either by ionic dissolution of the thiol or by formation of H*,

$$RSH + Au \Rightarrow RSAu^{-} + H^{+} \qquad [1.15]$$

$$RSH + Au \Rightarrow RSAu^{-} + H^{*} \qquad [1.16]$$

Based on the electrochemical data, the reaction [1.16] is favored significantly over the reaction [1.15]. The role of H* is different in the two most likely desorption reactions:

$$2RSH_{(solv)} + 2Au_{(s)} \Leftrightarrow 2RSAu_{(s)} + H_2 \qquad [1.17]$$

$$2RSAu_{(s)} \Leftrightarrow RSSR_{(solv)} + 2\,Au \qquad [1.18]$$

For the reaction $2H^* \rightarrow H_2$, ΔH= -104 kcal/mol, and for $H^* + Au\,(s) \rightarrow (HAu(s))^*$, $\Delta H \cong$ -2 kcal/mol. Therefore, the formation of molecular hydrogen will be thermodynamically favored over dissolution of H* into the Au matrix.

Three steps are involved in the formation of the monolayer of thiols on gold: the breakage of the SH bond, the formation of the Au-S bond, and the fate of H* as discussed above. The bond dissolution energy for the RS-H bond is given as ~87 kcal/mol, the RS-Au bond energy is ~ -40 kcal/mol, and $\frac{1}{2}(2H^* \rightarrow H_2)$ at –52 kcal/mol dominates over the Au matrix adsorption of H*. The calculated heat of reaction [1.18] is –5 kcal/mol, while the heat of the reverse reaction is +5 kcal/mol, if all reactants remain available. Similarly, the reaction to form RSSR involves the breakage of two RS-Au bonds (40 kcal/mol each) and the formation of a RS-SR bond (~74 kcal/mol for disulfide bond cleavage), giving a net heat of desorption of about +6 kcal/mol. Therefore, the adsorption reaction is thermodynamically favorable over the desorption process for thiol-gold system although the enthalpic contributions to the formation of these monolayers do not provide a complete picture (Karpovich, 1998).

The inter-chain forces, mainly van der Waals forces between adjacent methylene groups, amount to 1.4~1.8 kcal/mol, which add up to significant strength for alkyl chains of 10~20 methylenes, and play an important role in aligning the alkyl chains parallel to each other in a nearly all-trans configuration.

(3) Kinetics of SAM formation

Growth from solution is the traditional route for the preparation of SAMs, typically by immersing the metal substrate into an ethanolic solution of alkanethiol for a certain period of time. Kinetic studies of alkanethiol adsorption onto Au(111) surface have shown that in

relatively dilute solution (10^{-3} *M*), two distinct adsorption kinetics can be observed: a very fast step, which takes a few minutes, by the end of which the contact angles are close to their limiting values and the thickness is about 80~90% of its maximum, and the slow step, which lasts several hours, at the end of which the thickness and contact angles reach their final value. The initial step is diffusion-controlled Langmuir adsorption, strongly dependent on thiol concentration. The second step can be described as a surface crystallization process, where alkyl chains get out of the disordered state, and form a two-dimensional crystal. The kinetics of the first step is governed by the surface-head group reaction; on the other hand, the kinetics of the second step is related to chain disorder, chain-chain interaction and the mobility of chains (Bain, 1989a).

Based on the *in-situ*, real-time data derived with QCM (Karpovich, 1998), however, the assembly of alkanethiol/gold monolayers can reach a steady-state condition in a short time (seconds). Early studies of SAM formation reported that monolayer-forming reactions required hours or days to achieve completion (Bain, 1989a; Troughton, 1988; Truong, 1996). This discrepancy is related to the secondary properties brought about by the structural annealing of monolayer aliphatic chains, such as thickness, IR peak, or contact angle measured in *ex situ* studies. The structural annealing process proceeds in a slower rate than the adsorption of the thiol head group to the gold substrate. But Sastry (2000) reported a different time frame for the adsorption. The mass uptake with time curve derived by *in situ* QCM measurement indicates an initial rapid chemisorption of the ODT molecules (~20 minutes), followed by slower adsorption, which stabilizes within nearly 2 hours. The final steady state mass loading of 205 ng/cm^2 corresponds to an average molecular area of 23 Å^2, and a refractive index of 1.46 for ODT film can be calculated.

There is some recent evidence for cooperative interactions between head and tail groups, and between solvents and tail groups in the formation of SAMs. The adsorption kinetics depends on thiol concentration, which can be expressed by the Langmuir adsorption isotherm,

$$\frac{d\Theta}{dt} = k_a(1-\Theta)C - k_d\Theta \qquad [1.19]$$

where Θ is the fraction of available sites, and k_a and k_d are the adsorption and desorption rate constants, respectively. C is the thiol concentration, and t represents the time.

It is found that aliphatic chain annealing is also dependent of thiol concentration (Karpovich, 1998). For adsorption from dilute solution (in the range of 0.1 *mM* to 0.01 *mM*), there is a sufficient steady-state concentration of unoccupied gold sites, where free spaces exist for the aliphatic chains to reorient and isomerize to achieve their lowest energy conformation. For an adsorption from higher concentration, essentially a full monolayer is adsorbed at the outset; the steady-state concentration of free gold sites is too low to allow efficient aliphatic chain annealing.

(4) Effect of chain length, headgroup, solvent and temperature

Bain, et al. (1989b) studied the effect of the head group on monolayer formation on gold. Only sulfur and phosphorus exhibit a strong interaction with the gold substrate that promoted the formation of a closed-packed, ordered monolayer. Alsten (1999) reported the SAM formation of alkyl phosphonic acids on common engineering metals such as steel, stainless steel, aluminum, copper, and brass. *α,ω*-metal biphosphonate SAMs are fairly receptive to complexation by organic acids and acid-containing polymers such as fluoropolymers and ethylene-*co*-methacrylic acid, giving a surprising durability of polymer/SAM/metal interfaces.

The chain length affects the thickness and the contact angle of SAMs of *n*-alkanethiol ($CH_3(CH_2)_nSH$) on gold (Porter, 1987). There is a linear relationship between the thickness and the chain length with a slope of 0.56 Å/CH_2 and 1.5 Å/CH_2 for shorter chain (n=1~9) and longer chain (n=9~21), respectively.

Ethanol is suggested as the preferred solvent for the formation of alkanethiol SAMs. Bain, et al. (1989b) studied the effect of various solvents on the formation of *1*-hexadecanethiol monolayers. No considerable solvent effect on the thickness and contact angle was found. However, alkanes are not recommended as favorable solvents because of their tendency to incorporate into the two-dimensional system. Practically, the solubility properties of the alkanethiol derivatives dictate the choice of solvent. Kokkoli and Zukoski (1999) have found that solvents alter interactions between SAMs surfaces by changing the wetting properties of the surface. Adhesive forces measured with AFM decrease with solvent dielectric constant and vary monotonically for mixtures of water and ethanol. A newly filed US patent disclosed a method with compressed CO_2 as a solvent for forming SAMs of semi-fluorinated sulphur-containing

compounds (Fukushima, 2002). The benefits of using CO_2 as a solvent include good molecular packing density and relatively fast formation of SAMs.

Volmer (1989) studied the adsorption of *n*-propylmercaptan on a clean iron surface under ultrahigh vacuum with XPS. The mercaptan does not react at –196 ^{o}C but covers the surface in the form of a bulk condensation film. At –150 ^{o}C the mercaptan is chemically bound onto the surface and the Fe-S bond is quite heteropolar, S being charged negatively. At 25 ^{o}C, however, the mercaptan decomposes into segregated sulfur and hydrocarbons. But this is not true for the adsorption in solution, where only sulfur is able to replace water molecules or sulfur may react with iron atoms not attached to oxygen (Stratmann, 1995).

1.2.4.4 Structure and Properties of Thiol Films

(1) Structure of Thiol Films

The structure of thiol SAMs is determined by the interactions of sulfur head group and metal substrate, the interchain, and the interterminal groups (Ulman, 1991). These interactions determine the binding strength of head groups and substrate, the packing of the chain, and the arrangements of the surface terminal groups. *X*-ray or helium diffraction, IR, AFM, QCM, ellipsometry, and NMR are the commonly used techniques to characterize the structure of SAMs.

The first AFM study of thiol SAM was reported by Alves, et al (1992). AFM images of *n*-alkanethiol revealed a hexagonal lattice with a lattice constant of 5.1±0.3 Å. Butt, et al. (1993) imaged octadecanethiol (ODT) adsorbed on a sputtered gold surface, and found the surface periodicity of the SAM as well as various surface defects in the monolayers. These defects included curved lattices due to the local curvature of the gold substrate and point defects such as a single molecule sticking out or missing from the SAM. High-resolution images of SAMs can be readily obtained in liquids with AFM. From the AFM images of ODT/Au(111) acquired in *2*-butanol by Liu, et al. (1998), in addition to the long-range order, a step of 2.4 Å in height, which corresponds to the substrate defects, and 2.4 Å deep depression were clearly observed. These depressions are probably caused by dissolution of Au during thiol adsorption, and are often referred to as *etch pits*. They are randomly distributed in the flat Au(111) areas with 20 to 200Å lateral dimension. Cavalleri, et al. (1996) observed small depressions of similar dimensions on thiol-covered gold surface with STM measurement. They suggested that these defects can be healed by heating the monolayer up to 77~97 ^{o}C .

Diffraction and spectroscopic studies have revealed that the alkyl chains are tilted ~30° from the surface normal, and there are as many as twelve equivalent azimuthal orientations along which molecules could tilt (Porter, 1987; Nuzzo, 1990a). As a result, domains are present within the monolayer, and each domain possesses a region with a single preferred tilt angle. These domains are also visible in AFM images (Alves, 1992; Liu, 1998).

Early diffraction studies of the structure of alkanethiol SAMs on gold (Chidsey, 1989, 1990; Strong, 1988) reported a hexagonal ($\sqrt{3} \times \sqrt{3}$) R30° structure with respect to Au(111), corresponding to a intermolecular spacing of ~5 Å and a area per molecule of 21.6 Å^2, which is significantly larger than the cross section of a hydrocarbon chain (18.4 Å^2). This suggests that the chain axis should be tilted so that the hydrocarbon chain-chain packing can be maximized. The tilt angle should be (18.4/23.6) ~32°. This is close to the value of the IR studies (Nuzzo, 1990a), and also consistent with the direct measurement by *X*-ray diffraction (Fenter, 1997, 1998).

IR study (Nuzzo, 1990a) established the molecular orientation of an average single chain, with structure consisting of *all-trans* zigzag chain canted by ~34° from the surface normal with the plane defined by the trans segments rotated by ~55°. STM images presented a c(4×2) superlattice of the ($\sqrt{3} \times \sqrt{3}$) R30° structure (Poirier, 1994). This rectangular unit cell has the dimensions 9.994 Å×8.655 Å, which is four times larger than that of ($\sqrt{3} \times \sqrt{3}$) R30° lattice, suggesting that it contain four molecules.

Based on *X*-ray diffraction study (Fenter, 1997), there are two distinct regimes of the tilt angle, which for n≤14 is systematically ~3° greater than for n≥16. In addition, the tilt direction tends to shift away from the next-nearest neighbor (NNN) towards the NN direction for shorter chain lengths.

As for headgroup structure, the sulfur position is found to deviate from the hexagonal ($\sqrt{3} \times \sqrt{3}$) R30° symmetry (Fenter, 1994). S-S spacing is ~2.2 Å instead of 5 Å for a perfect hexagonal ($\sqrt{3} \times \sqrt{3}$) R30° symmetry, implying the formation of a dimerization.

Pflaum, et al. (2002) investigated the structure and the electronic properties of CH_3- and CF_3-terminated alkanethiol monolayers on Au(111) with STM and surface *X*-ray scattering. At full coverage, the former forms long-range ordered domains of a ($\sqrt{3} \times \sqrt{3}$) R30° and a ($2\sqrt{3} \times \sqrt{3}$)

R30^{o} standing-up phase, while CF_3-terminated monolayers form a standing-up phase of hexagonal symmetry that exhibits no long-range order at room temperature.

(2) Mixed SAMs

Interestingly, the surface properties can be tailored by mixing appropriate ingredients, thus creating multi-component SAMs, or mixed SAMs. For instance, mixing hydrophobic CH_3-terminated and hydrophilic HO-terminated thiols can attain a SAM surface with desirable wetting property. In the same way, a rough, heterogeneous surface can be fabricated by mixing thiols with different chain length. Figure 1.9 illustrates two mixed SAMs. The mole fraction of each molecule in the SAM can be controlled via the molar ratio of the two molecules in the solution, as well as the deposition conditions (Folkers, 1994; Ulman, 1996b).

Zerulla, et al. (1998) attempted to create mixed thiol films with two structurally and chemically different thiol species, namely, the aliphatic hexadecanethiol (HDT) and the aromatic *2*-mercapto-benzothiazole (MBT). XPS shows that HDT can displace MBT from gold surfaces. In contrast, MBT cannot replace the adsorbed alkanethiol layer. The creation of mixed films starts with a partial coverage of HDT, followed by the MBT, which can assemble to the uncovered surface without disturbing the alkanethiol.

Barrena, et al. (2001) compared the frictional and structural properties of single component forms of alkanethiols (C_{12}, C_{16}) and their mixed films with AFM measurement. For single

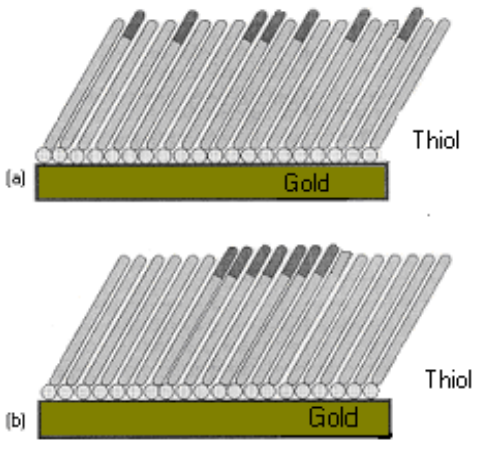

Figure 1.9 Two mixing SAMs, exhibiting (a) homogeneous mixing, and (b) phase separation. Differences in chain length and terminal groups are shown (Finklea, 2000).

component films, the friction increases monotonously with the applied load. In contrast, the friction force of the mixed films increases at a high rate at first and then at the same rate as in single component films. They proposed that the initial fast increase in friction is due to an energy dissipation mechanism based on the formation of gauche defects at the protruding ends of the long thiol molecules.

(3) Surface energy of various tail groups

Both high- and low-energy organic surface on metal substrates can be produced by the means of modifying the tail group present in adsorbing thiols, sulfides and disulfides. The surface energy of SAMs is related to various interfacial properties, such as wetting, friction, adhesion, and adsorption. Therefore, it is fairly critical to their applications in wetting control, corrosion inhibition, adhesion, and bio-related applications, etc.

Table 1.4 presents the wetting property of alkyl-based monolayer containing various tail groups (Laibini, 1998). For example, SAMs formed from $HS(CH_2)_nX$ may generate surfaces with high (X=COOH), intermediate ($X=OCH_3$), or low($X=CH_3$) surface free energy. Polar

Table 1.4 Contact angle of SAMs on gold formed from alkanethiol ($HS(CH_2)_nX$) with various tail groups (Laibini, 1998)

Tail group (X)	n	Advancing contact angle (degrees)	
		water	hexadecane
High-energy surface			
COOH	10	<15	<10
	15	<15	<10
OH	11	<15	<15
	16	<15	<10
	22	25	<10
Intermediate-energy surface			
OCH_3	11	74	35
	16	85	44
OCH_2CH_3	11	96	43
	16	99	49
Low-energy surface			
CH_3	17	115	48
	21	117	49
$CH=CH_2$	17	107	39

terminal groups of high-energy surface (-COOH, -OH, -NH_2, etc.) can provide reactive sites for further derivatization of a monolayer surface, and act as a type of coupling agent or adhesion promoters that link the solid substrate and various organic or biological species. For ether-terminated alkanethiols (e.g., $CH_3(CH_2)_mO(CH_2)_nSH$), four carbon units (~5 Å thick) are sufficient to screen interaction between a polar contacting liquid and the underlying polar ethereal oxygen. Due to their dense packing, robust behavior, and hydrophobic nature, SAMs of methyl-terminated alkanethiol can provide barriers that prevent interaction between redox and the underlying substrates.

Table 1.5 shows the critical surface tension of various organic surfaces. Surface energy increases in the order of fluorocarbon, hydrocarbon, chlorocarbon and nitrated hydrocarbon surface.

(4) Effect of temperature on structure and thermal stability

An *X*-ray diffraction study revealed that the phase transition of a full-coverage decanethiol SAM on Au(111) is at about 100 ^oC, much higher than in the bulk (-26 ^oC). It suggests that the crystalline structure is stabilized by the chemical bond to the substrate (Schreiber, 1998). The phase behavior is dependent of the coverage and the chain length. Generally, lower coverage makes melting (disordering) easier because more space is available for disordering. The melting temperature will increase with longer chain length.

With increasing temperature, defects like gauche conformations will be accumulated, thus reducing the order in the monolayer. Gauche defects are essentially quenched below –73 ^oC. At room temperature they reach a level of about 1% and increase further at higher temperatures (Nuzzo, 1990b).

According to the XPS and contact angle measurement conducted by Sung and Kim (2001), the monolayers of alkanethiol (C4, C8 and C16) on copper are stable in air up to 140 ^oC, but begin to desorb above 160 ^oC through the oxidation reaction of thiolate to sulfonate, with the alkyl chains remaining intact. Following the desorption, the copper surfaces are oxidized to CuO or $Cu(OH)_2$ at about 180 ^oC. Nishida, et al. (1996) have observed that ODT monolayers adsorbed on Au(111) were subjected to the desorption of entire chains at 177 ^oC, indicating that the desorption takes place through cleavage of the Au-S bonds. In contrast, alkylsiloxane

Table 1.5 Critical surface tension of common organic surfaces (Tillman, 1988)

Surface Constitution	Critical Surface Tensions, γ_c mJ/m^2, at 20 ^{o}C
Fluorocarbon surfaces	
-CF_3	
-CF_2H	15
-CF_3 and CF_2-	17
-CF_2-	18
-CH_2-CF_3	20
-CF_2-CFH-	22
-CF_2-CH_2-	25
-CFH-CH_2-	28
Hydrocarbon Surfaces	
-CH_3 (crystal)	22
-CH_3 (monolayer)	24
-CH_2-	31
-CH_2- and ..CH..	33
..CH.. (phenyl ring edge)	35
Chlorocarbon Surfaces	
-CClH-CH_2-	39
-CCl_2-CH_2-	40
=CCl_2	43
Nitrated Hydrocarbon Surfaces	
-CH_2ONO_2 (crystal) [110]	40
-$C(NO_2)_3$ (monolayer)	42
-CH_2NHNO_2 (crystal)	44
-CH_2ON_2 (crystal) [101]	45

monolayers on SiO_2 are more thermally stable, which begin to decompose at 470 ^{o}C through the cleavage of C-C bonds, resulting in a gradual decrease in chain length (Kluth, 1997).

1.2.4.5 Applications of Thiol Film in Corrosion Protection

SAMs formed on the metal surface act as a close-packed, strongly bound thin film. They have a potential for corrosion protection of metal substrates *via* the barrier effect. It is also possible to modify the surface functionality to improve the compatibility to topcoat.

Zamborini and Crooks (1998) studied the ability of *n*-alkanethiol SAMs to protect Au from corrosion in aqueous Br^- solutions by electrochemical measurement. It was found that the crystalline, highly ordered SAMs were degraded to a disordered state with molecules oriented parallel to the surface plane after exposure to corrosive media. For SAMs containing the same

terminal functional group, corrosion resistance increased as the SAM thickness increased. For SAMs with the same thickness but different terminal functional groups, the end groups resulting in the great corrosion resistance followed the order OH>COOH>CH_3, although hydrophilic HO- or COOH-terminated SAMs were generally more defective. The hydrophilic SAM-modified gold surfaces corroded smoothly in a layer-layer fashion while the methyl-terminated, hydrophobic SAM-coated surfaces underwent a localized corrosion (i.e., *pitting*).

Scherer, et al. (1997) reported their *in-situ* STM and electrochemical study on the corrosion of alkanethiol (n=8 and 16) covered Cu (100) in 1 *mM* HCl solution. They concluded that the SAM could inhibit the nucleation of corrosion sites as well as the growth of existing defects. SAM-coated copper started corrosion with the increase of surface roughness and growth of initial pits. It was different from the corrosion behavior of bare Cu (100), which was dissolved in a strict layer-by-layer mode. Apparently, the lateral growth of the holes was significantly inhibited by the SAM on the surrounding surface, demonstrating the stabilization influence of the strongly bound thiol adlayer. Azzaroni, et al. (2000) also found that the SAM of alkanethiol (n=12) was able to hinder copper oxide formation and copper dissolution in electrolyte solution containing chloride anions. This ability depended on the electrode potential and the concentration of aggressive anions.

Jennings, et al. (1996, 1998) studied the SAM of alkanethiols with long carbon chains ($C_{18}H_{37}SH$ and $C_{22}H_{45}SH$) on copper to provide corrosion resistance in aqueous environments. They used evaporated copper films on silicon wafers as the substrate and measured the change in water contact angles. It was suggested that the monolayer films provide a barrier against water penetration. The corrosion rate of copper varied with the film thickness, which depended on the chain length. For example, the thickness will increase from 10 Å to 30 Å by using longer-chained thiol (C_{22}) rather than shorter one (C_8). In order to increase the thickness, they tried to construct a multilayer assembly on copper surface. Mercaptoalcohol ($HS(CH_2)_nOH$, n=11, 22) was used for the first layer, and an alkyltrichlorosilane ($CH_3(CH_2)_{17}SiCl_3$) for the second layer through the reaction between hydroxyl group and siloxane. However, the bilayer films were not effective in improving the corrosion-inhibition abilities of the assembled coating beyond those related to SAMs derived from *n*-alkanethiols.

A monolayer coating of *1*-octadecanethiol (ODT) on an iron electrode gave an increase in protective efficiency to 76.3% (as calculated from impedance measurements) in a 0.5 *M* NaCl

solution. When an iron surface was coated first by *11*-mercapto-*1*-undecanol (MUO, $HO(CH_2)_{11}SH$) and then coated by octyltriethoxysilane, its protective efficiency was increased to 88.0% due to crosslinking polymerization (Nozawa, 1997 and 1999). When the MUO coated surface was coated again with *1,2-bis*(triethoxysilyl) ethane (BTSE) and then with 5×10^{-4} *M* octadecyltriethoxysilane, the efficiency increased to 98.1%. XPS studies revealed that the two-dimensional polymer film could protect iron from atmospheric corrosion (Aramaki, 1999).

Teneichi, et al. (2001) modified the MUO SAM with alkylisocyantes ($C_nH_{2n+1}NCO$) for the protection of copper in an aerated solution of 0.5 *M* Na_2SO_4. Protective efficiencies of 94.7% and 95.4% were obtained with octyl- and octadecyl isocyanate, respectively. Ishibashi, et al. (1996) studied oxygen permeability of alkanethiol SAMs adsorbed on copper electrodes. This protective film acted as barrier to oxygen diffusion from aerated aqueous solution since the cathodic process of copper corrosion was suppressed. Interestingly, hydrated oxygen molecules could enter into MUO SAM because of the wettability on the film surface.

Quan, et al. (2001) found that the pure films derived from Schiff bases, such as *N-2*-hydroxyphenyl-(*3*-methoxy-salicylidenimine), *N-2*-hydroxyphenyl-(salicylidenimine), *N,N'*-o-phenylene-bis-(salicylidenimine), on copper surface showed some defect sites. When the film was modified with *1*-dodecanethiol, the quality and corrosion resistance of the mixed films improved markedly.

Grundmeier, et al. (1998) showed that thiol (R-SH) coated on bare iron promoted the adhesion of ultrathin (<10 nm) plasma polymers. The stability of the composite coating increased substantially.

In US patent No. 6,102,521, Halko, et al. (2000) disclosed a technique of treating a gold-plated orifice of ink-jet pen with thiol-type SAMs to control wettability of the surface in order to reduce the accumulation of residual ink and inhibit corrosion and contamination of the plate while presenting a uniform surface for the ink.

In US patent No. 6,183,815 B1, Enick and Beckman (2001) claimed a method for coating a metal surface with amide thiols solution to produce a gas-, water-, oil- and corrosion-resistant outer layer. The preferable compounds have a general formula, $F(CF_2)_mCONH(CH_2)_nSH$, where n and m are each 2~20. They are effective on many metal including gold, silver, nickel, copper, brass, tin, iron, etc., but not effective for aluminum and its alloys.

1.3 TEST TECHNIQUES FOR ORGANIC COATINGS

1.3.1 General Information

Corrosion resistance and paint adhesion are two of the most important properties of conversion coatings and other type of protective coatings. Because of the complexity of corrosion and adhesion phenomena, it is not surprising that there exist so many test methods. Overall, corrosion data can be collected from service experiences, pilot plant tests and laboratory tests. Without doubt, the most reliable test data are based on service experience. However, laboratory test can often offer the flexibility of a broad range of standard and fundamental corrosion measurement. Laboratory tests also offer the unique advantages over in-plant tests: acceleration of results through variation of parameters. Proper test method should be decided in terms of the test purpose, the type of materials and the service environments.

1.3.2 Accelerated Corrosion Tests

1.3.2.1 Standard Salt Spray Test (SST)

The most widely used standardized laboratory corrosion test is defined in ASTM B117, Test Method of Salt Spray (Fog) Testing. This is an accelerated corrosion test conducted in a cabinet, consisting of a fog chamber, a saltwater reservoir, a supply of compressed air, one or more atomizing nozzles, specimen supports, heating and control system. The salt solution of 5% concentration should be prepared by using sodium chloride with total impurities less than 0.3% and the purified water as stated in ASTM Specification D1193. The compressed air should be maintained between 10 to 25 psi. The temperature over the exposure zone in the chamber should be maintained at 35+1.1-1.7 ^{o}C, and the average fog amount collected over 80 cm^2 of horizontal area should range from 1.0 to 2.0 mL of solution per hour. The cut edges of painted or coated specimen should be properly protected with paint, wax or tape to avoid the galvanic effect. The specimen should be supported or suspended between 15 and 30^{o} from the vertical and preferably parallel to the principal direction of flow of fog through the chamber.

In spite of severe criticisms regarding the lack of correlation with service experiences (Appleman, 1982 and 1992; Lee, 1984; Skerry, 1991), this method is still widely accepted as an effective approach for predicting corrosion resistance performance property of coated materials and for comparing different materials or finishes. A number of variations of the salt spray test have been standardized for specific purposes. These include ASTM B287, Method of Acetic

Acid-salt (fog) testing; ASTM B368, Method for Copper-Accelerated Acetic acid-salt spray (fog) testing (CASS Test); ASTM G 43, Method of Acidified Synthetic Sea water (fog) testing; ASTM G 85, Practice for Modified Salt Spray (Fog) Testing, which includes a salt/SO_2 test and "Prohesion" Test.

More details for the salt spray test should be determined between supplier and customer of a material.

1.3.2.2 Cyclic Corrosion Test (CCT)

In order to duplicate specific corrosion mechanisms more closely, modern accelerated corrosion testing often involves cyclic tests, which include periodic salt spray exposure combined with exposure to other conditions such as high and low humidity, temperature extremes, mechanical forces, etc. (Baboian, 1995; Simpson, 1991). Filiform corrosion, for instance, can be produced by exposure to salt spray and then to 70~90% humidity (ASTM D 2803). Blistering of coatings (*scab corrosion*) can be achieved by exposure to salt spray, humidity, and cold (ASTM D 2933).

Another testing regimen called "*Prohesion*" has been reported to correlate better with actual performance than standard salt spray test (Timmins, 1989; Cremer, 1989). It is a modified salt fog exposure procedure with emphasis on adhesion evaluation of thin film. Scribed panels are sprayed with the mixed solution of 0.4% ammonium sulfate and 0.05% NaCl for 24 hours, six 3-hour periods alternating with six 1-hour drying period using ambient air.

GM9505P, Performance of Substrate and/or Coatings Through Environmental Cycling, and GM9540P, Accelerated Corrosion Test are two cyclic tests extensively used to simulate the automotive environment. The former involves cyclic salt spray exposure while the latter involves periodic spray application and humidity cycling. A typical "scab" test is recommended on painted steel panel with 20 corrosion testing cycles involving subsequent exposures in salt fog, humidity, and exposure under controlled temperature (-13 ^{o}C and 60 ^{o}C) (Porter, 1994).

Corrosion damage following the salt spray test can be assessed by a variety of techniques. Visual appearance of the specimen can provide the most important information. ASTM D 1654 also gives a standardized rating system for evaluating painted or coated specimen subjected to corrosion environment. Mass loss measurement can be used to qualify test results for uniform corrosion.

1.3.3 Electrochemical Methods

1.3.3.1 Tafel Test

Metallic corrosion is usually an electrochemical process, which involves oxidation reactions in anode and reduction reactions in cathode as represented in equation 1.20 and 1.21. Electrons flow between the anodic and the cathodic area through an ionic conduction path of an electrolyte can be interpreted as a corrosion rate.

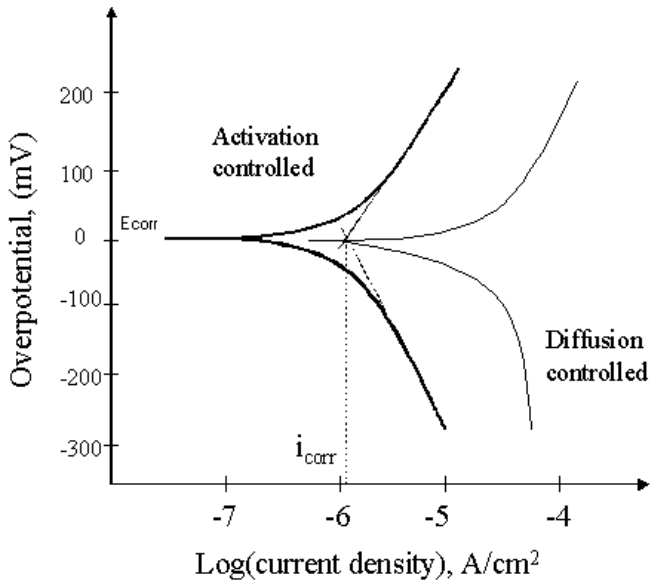

Figure 1.10 Typical Tafel plot for both activation and diffusion controlled corrosion rates. i_{corr} is the corrosion current, an indicator of corrosion rate, E_{corr} is the corrosion potential.

Oxidation of metal in water:

$$M = M_n^+ + ne^- \qquad [1.20]$$

Reduction of oxygen in aerated neutral or alkaline media:

$$O_2 + 2H_2O + 4e^- = 4OH^- \qquad [1.21]$$

No external electrical current flows to or from a test electrode when it is at open circuit potential (OCP), even when the electrode is corroding and thus has a corrosion current, i_{corr}. An external potential must be applied to a test electrode to move its potential away from OCP and

therefore obtaining an electrical current that can be measured. The Butler-Volmer equation relates electrical current to changes in metal potential caused by an overpotential (Bard, 1980):

$$i = i_{corr} \{\exp(-\alpha nF\eta/RT) - \exp((1-\alpha)nF\eta/RT)\} \quad [1.22]$$

Where, i_{corr} is the corrosion current density (A/cm^2), that occurs when electrode is at its OCP;

i is the external current density, flowing to or from an electrode because of an applied potential;

η is the test electrode overpotential and is the difference between OCP and applied potential;

n is the number of electrons in the anodic half reaction;

α is a coefficient having values that range from 0 to 1;

R is the ideal gas constant, 1.98 Cal/mol.K;

F is Farady's constant, 96,500 C/eq.;

T is temperature in degrees Kelvin.

Tafel scan begins at approximately –250 mV from OCP and ends at approximately +250 mV from OCP, and Tafel plot spectra are plotted as potential versus log value of current density, as shown in Figure 1.10. Corrosion rate (or corrosion current, i_{corr}) can be read directly from a Tafel plot.

1.3.3.2 Electrochemical Impedance Spectroscopy (EIS)

It is generally accepted that electrochemical impedance spectroscopy is a very useful technique for the investigation of the corrosion performance of metallic coatings and organic barrier coatings (Mansfeld, 1982 and 1985; Kendig, 1983 and 1990; Scully, 1989). This method does not accelerate the corrosion reaction and is nondestructive. The technique is quite sensitive to changes in the resistive-capacitive nature of coatings as well as electrochemical interface. In this technique, typically a small-amplitude sinusoidal potential perturbation (usually within ± 5 mV) is applied to the working electrode at a number of frequencies, usually ranging from mHz to 100 KHz.

(1) Impedance model for a corroding metal/electrolyte interface

When an A.C. signal is impressed on a metallic electrode immersed in an electrolyte solution, a time-dependent electrical double layer is set up. Because no net current flows, the

system reaches a steady state after a few cycles. The interface behaves as a simple electrical circuit (Figure 1.11), which consists of the ohmic resistance (R_Ω) in solution, and the impedance of the Faradic process across the interface (R_f) and the double layer capacitance (C_{dl}). The circuit given in Figure 1.11 is known as Randles circuit. For activation-controlled reactions, R_f is equal to the resistance to charge transfer R_{ct}, also referred to as polarization resistance, R_p. In this case, the impedance (Z) of the overall circuit is given by the following equation,

$$Z = \left(R_\Omega + \frac{R_p}{1+\omega^2 R_p^2 C_{dl}^{\ 2}} \right) - j\frac{\omega R_p^2 C_{dl}}{1+\omega^2 R_p^2 C_{dl}^{\ 2}}$$
$$= Z' + Z'' \qquad [1.23]$$

Where ω is the angular frequency (=2πf where f is AC frequency in Hz). The first term (R_Ω) represents the uncompensated solution resistance, the second term represents the contribution from R_p, and the third term represents the imaginary impedance. Thus, the sum of the first two terms represent the real impedance (Z'), and the third term represents the imaginary impedance (Z''). A plot of Z'' vs. Z' is known as a complex plane plot or *Nyquist plot*. For the Randles circuit, the plot gives rise to a semi-circle as shown in Figure 1.12. At large value of ω, the semi-circle intercepts with the Z' axis at R_Ω. As ω approaches zero, the semi-circle intercepts

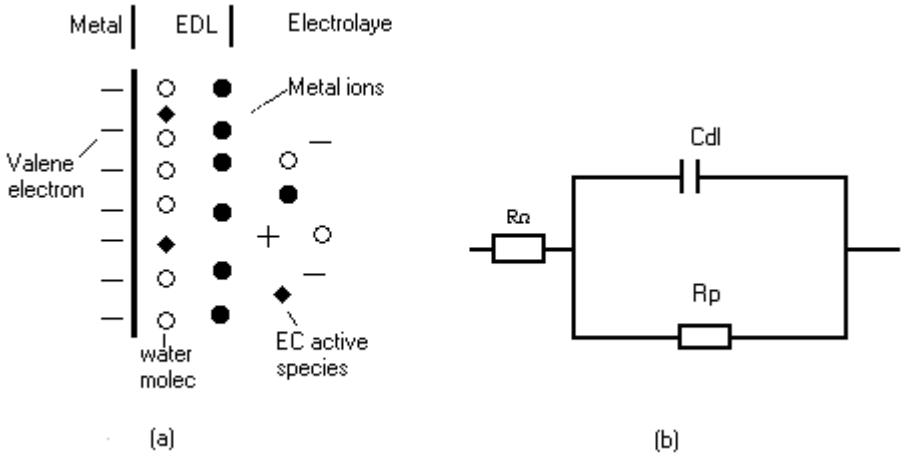

Figure 1.11 Electrical interface structure and equivalent circuit model simulating a simple corroding metal/electrolyte interface (Englehart,1974; Tait, 1994). R_Ω is the solution resistance, R_p is the polarization resistance (similar to Rct, a charge transfer resistance), C_{dl} is the double layer capacitance.

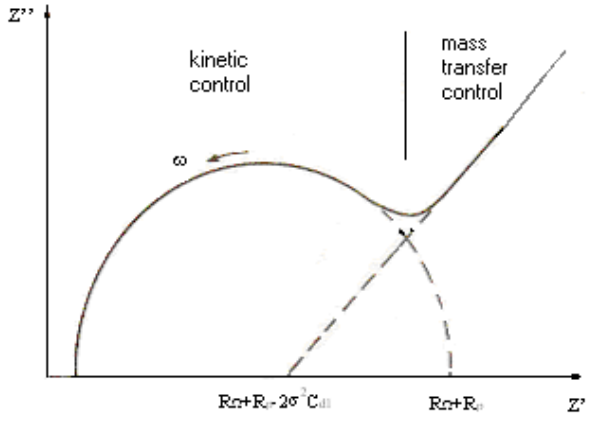

Figure 1.12 Nyquist plot of impedance in the complex plane of the electrochemical system corresponding to the circuit model in Fig. 1.11. σ is a parameter representing diffusion of electrolyte, ω is the angular frequency (ω=2πf where f is AC frequency in Hz).

with the Z' axis at $R_\Omega+R_p$. If the electrochemical reaction is mass transfer controlled, a straight line is obtained as shown in Figure 1.12. The interception with the Z' axis gives $R_\Omega+R_p-2\sigma^2C_{dl}$, where σ is a complex function of the concentration of oxidant and reductant, and their diffusion coefficients.

(2) Impedance model for a coated metal panel with defects

Electrochemical impedance spectroscopy is capable of discriminating the resistive properties of the coatings because of its ionic and/or electronic conductivity and the capacitive nature of the coatings due to its dielectric constant, area, and thickness. EIS data can provide adequate information regarding the degradation, porosity and interface delamination of the coating system on metal substrates.

Figure 1.13 shows an impedance circuit model for coatings. Although this model contains more elements than the model shown in Figure 1.11, frequency regimes in which impedance information is primarily due to the coating capacitance or coating resistance can be separated from one another and analyzed independently by using a broad frequency bandwidth.

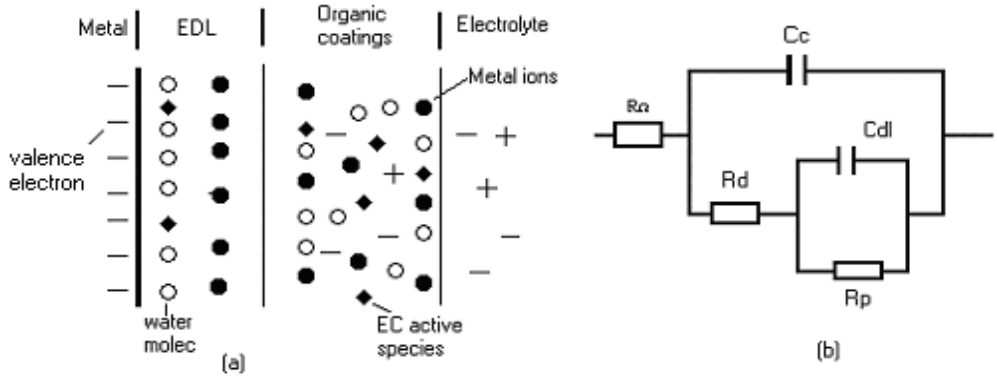

Figure 1.13 Electrified interface structure and equivalent circuit to simulate a coated metal panel with a defect (Englehart,1974; Tait, 1994). R_d is the coating defect (pore) resistance, C_c is the coating capacitance, R_p is a charge transfer resistance at the metal interface where water has penetrated.

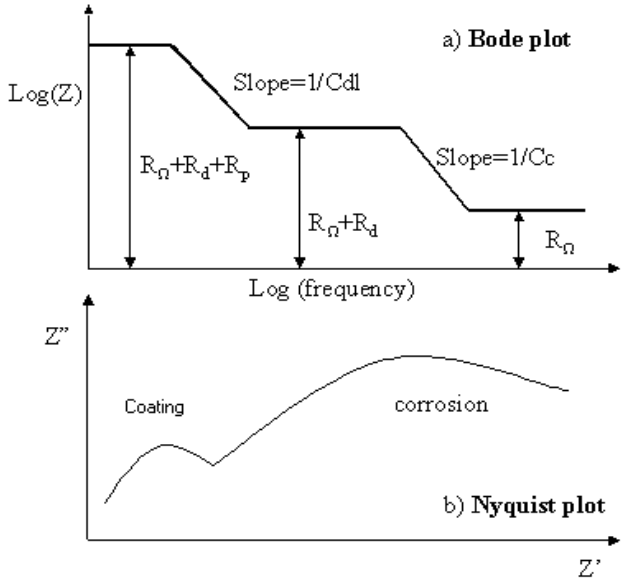

Figure 1.14 Schematic of (a) Bode plot, and (b) Nyquist plot of the equivalent electrical circuit model in Figure 1.13. These plots are idealized, a real plot from a coated metal system may be different.

Figure 1.14 represents a typical impedance plot of the simulated electrical circuit of a coated metal/electrolyte interface. It is realized that most paints and the double layers at the paint/metal interface do not behave like real capacitors; instead, they behave like constant phase element (CPE). The nonideal behavior is caused by the surface roughness of the metal, heterogeneity of the paint, the finite resistance of the paint, and even the formation of the oxide layers (Zhang, 1997). A CPE is defined as that its impedance (Z) obeys the following equation:

$$Z = Y(j\omega)^{-n} \qquad [1.24]$$

Where Y and n are constants. When a CPE describes a real capacitor, Y is equal to the inverse capacitance, and n is equal to 1. If n is equal to zero, the CPE is a resistor. Therefore, in the model shown in Figure 1.13, CPE 1 (C_c, Y_1 and n_1) describes the nonideal capacitive behavior of the paint including the pretreatment, and CPE 2 (C_{dl}, Y_2 and n_2) describes the nonideal capacitive behavior of the double layer formed at the interface. All the elements of an equivalent circuit model can be extracted by using a specifically written program such as EQUIVCRT, developed by Boukamp, B. A. of University of Twente, The Netherlands.

The film thickness can be determined for a given exposed area if the coating capacitance can be measured by impedance and if the dielectric constant is known (Baboian, 1995):

$$C = \frac{\varepsilon\varepsilon_o A}{d} \qquad [1.25]$$

Where, A = the surface area, cm^2,

D = the dielectric thickness, cm,

ε_o = the electric permittivity of a vacuum (8.854×10^{-12} F/m), and

ε = the electric constant of a coating.

The uptake of water in an organic coating can be estimated from the following equation (Kendig, 1983):

$$Vol.\%water = \frac{100\log(\frac{C_t}{C_o})}{\log(79)} \qquad [1.26]$$

Where C_t = the coating capacitance after some exposure time, and

C_o = the coating capacitance in time zero when the exposure begins.

The coating resistance can also be monitored as a function of exposure time. The permeation of ionic species through the coating or the presence of defects in the coating can cause a drop in coating resistance. The breakpoint frequency can be used for estimating the area fraction of physical defects in an organic coating (Scully, 1989; Kendig, 1990; Hack, 1991):

$$f_b = \frac{1}{2\pi\varepsilon\varepsilon_o\rho}\left(\frac{A_d}{A}\right) \qquad [1.27]$$

where ρ = the resistivity of the coating at the defect,

f_b = the breakpoint frequency of the coating after exposure,

A_d = the defect area, and

A = the total area.

1.3.4 Paint Adhesion

1.3.4.1 Tape Test

Paintability is another important property of a conversion coating. Good paint adhesion can generate a good corrosion resistance for the whole coating system. The most common procedure to measure paint adhesion is designated in ASTM D 3359 (Test Method for Measuring Adhesion by Tape Test), often referred to as *tape adhesion*. The test method involves using a cutting tool to scribe a series of cuts into the sample. Method A introduces a '×' cut, while Method B describes a crosshatch pattern. The next step is to apply a special pressure-sensitive adhesion tape onto the scribed panel. The tape is then rapidly removed, and the amount of coating that detaches is rated according to either descriptions or illustrations in a scale from '0' to '5'. The best rating is a '5'; the worst is a '0'. Weldon (2001) discussed the advantages and shortcomings of this test method in his recent book.

A similar test can be performed according to the standard GM 9071P, Crosshatch test. One hundred squares of 1.5 mm ×1.5 mm in the paint film are cut down into the base metal with a special tool. Immediately following crosshatching, the area is tested several times with adhesive tape until no more paint can be removed. The test results are expressed as the number of paint

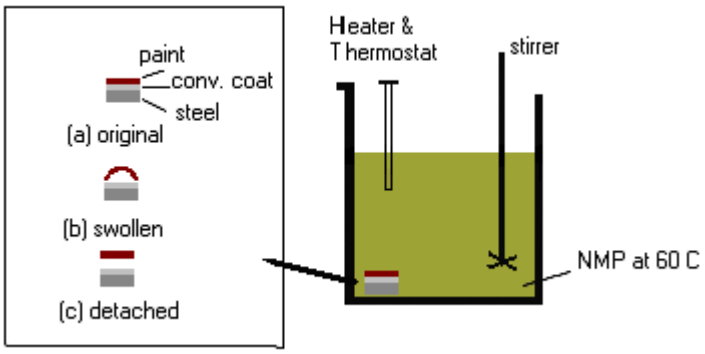

Figure 1.15 N-methylpyrrolidone (NMP) nondestructive adhesion test for paints (Van Eijnsbergen, 1994)

squares removed from the crosshatched area. This test may also be conducted after the water soak test. The panels are dried only superficially with blotting paper (Van Ooij, 1993b).

1.3.4.2 NMP Paint Retention Test (NMPRT)

Van Ooij's group has designed a new test for estimating the adhesion of paint to metal substrates (Van Ooij, 1982 and 1993b; Chidambaran, 1991). *N*-methyl pyrrolidone (NMP) was used as a swelling agent to induce interfacial shear stresses and break the bonds at paint/metal interface. In the NMP paint delamination or retention test, disks of 16 mm diameter (2 cm^2) were punched out of painted panels and then immersed in NMP held at 60 ^oC. The time when the paint had completely detached was recorded and referred to as the NMP paint retention time or NMPRT. The NMPRT value is believed to be a measure of the number or strength of the interfacial bonds such as hydrogen bonds, or, more generally, acid-base interactions. Paints that form covalent bonds cannot be removed by NMP. Therefore, this test is particularly useful for evaluating the paint performance on the surface modified by conversion coatings. Paint failures are most likely to occur at paint/conversion coating interface. Figure 1.15 is a schematic description of this test.

The paint performance can be evaluated by NMPRT value as follows:

(i) < 1 minute, very poor adhesion;

(ii) 1~10 minutes, poor to mediate adhesion;

(iii) 10~50 minutes, good adhesion;

(iv) >50 minutes, excellent adhesion.

1.3.5 Surface Characterization

1.3.5.1 Contact Angle Measurement and Surface Tension

Coatings or paints must come into intimate physical contact with the substrate in order to achieve a good adhesion. The process of a liquid spreading over and coming into intimate contact with a substrate is called *wetting*. To understand wetting and the factor that influence it, one must have an understanding of surface tension, or surface free energy. Surface tension is the excess free energy associated with molecules at the surface compared to molecules in the bulk of liquid or solid.

The surface tension of a liquid can be measured experimentally by such techniques as the Du Nouy ring method or the Wilhelmy plate method (Weldon, 2001). The surface tension of a solid surface can be determined indirectly through contact angle measurement of a liquid on the solid.

We have discussed the surface energy of a liquid or a solid as a whole in the previous sections. Actually, surface energy is consist of three components that are called Lifshitz-van der Waals γ_{LW}, Lewis acid γ^+ and Lewis base γ^- energies, respectively. The surface energy components of the solid can be experimentally measured according to Van Oss-Goods-Chandrey equation (Van Oss, 1994; Good, 1990):

$$(1+\cos\theta)\gamma_L = 2(\sqrt{\gamma_S^{LW}\gamma_L^{LW}} + \sqrt{\gamma_S^+\gamma_L^-} + \sqrt{\gamma_S^-\gamma_L^+}) \qquad [1.28]$$

Where, θ is the contact angle of a liquid on a smooth solid surface; γ_{LW}, γ^+ and γ^- are the nonpolar, acidic and basic component of surface tension, respectively. The subscript L and S denote liquid and solid, respectively.

If a contact angle is known for a liquid of known γ_L^{LW}, γ_L^+, γ_L^-, each equation will only have three unknowns, i.e., γ_S^{LW}, γ_S^+, γ_S^-. For a given solid surface, one can measure contact angles using three different liquids, as shown in Table 1.6, which will give three equations with three unknowns. By solving them simultaneously, it is possible to determine γ_S^{LW}, γ_S^+, and γ_S^-.
From the three components, one can find the surface tension of a solid by using Fowkes equation shown below (Van Oss, 1994; Good, 1990). γ_S^{LW} represents Lifshitze-van der Waals component of a solid (apolar or nonpolar surface tension), which occurs everywhere in a substrate; γ_S^{AB} is polar acid-base component of the surface tension, which may be monopolar or bipolar.

Table 1.6 Surface tension components of several liquids at 20°C in mJ/m^2 (Van Oss, 1994)

Liquid	γ_L	γ_L^{LW}	γ_L^{AB}	γ_L^+	γ_L^-
Hexane	18.4	18.4	0	0	0
Carbon Tetrachloride	27	27	0	0	0
1-Bromonaphthalene	44.4	44.4	0	0	0
Methylene Iodide	50.8	50.8	0	0	0
Benzene	28.85	28.85	0	0	2.7
Chloroform	27.15	27.15	0	3.8	0
Ethanol	22.4	18.8	2.6	0.019	68
Ethylene Glycol	48	29	19	1.92	47
Glycerol	64	34	30	3.92	57.4
Formamide	58	39	19	2.28	39.6
Water	72.8	21.8	51	25.5	25.5

$$\gamma_S = \gamma_S^{LW} + \gamma_S^{AB} = \gamma_S^{LW} + 2\sqrt{\gamma_S^+ \gamma_S^-} \qquad [1.29]$$

It is useful to understand the surface tension components and the acid-base interaction. It is known that complementary surface tensions are favorable for adsorption: acidic surface likes to interact with basic coating materials, and *vice versa*. From the practical point of view, the acid-base interaction theory can be used to develop the novel coating composition and explain the mechanism of coat/substrate interaction. For example, a coating with acidic property will be favorable for the zinc surface that is weakly basic with pronounced γ^- value. The surface tension components of selected liquid and solid are given in Table 1.6 and Table 1.7 (Van Oss, 1994).

Table 1.7 Surface tension components of the selected solids at 20°C in mJ/m^2 (Van Oss, 1994)

Solid	γ_S	γ_S^{LW}	γ_S^{AB}	γ_S^+	γ_S^-
Teflon	17.9	17.9	0	0	0
Polyethylene	33	33	0	0	0
Polyethylene Oxide	43	43	0	0	64
Nylon	37.7	36.4	1.3	0.02	21.6
Talc	36.6	31.5	5.1	2.4	2.7
Calcite Crystal	57	40.2	16.8	1.3	54.4
Silica Glass	49.8	34	15.8	1	64.2
Coal	39.8	39.8	0	0	2.5

1.3.5.2 Fourier Transform Infrared Spectroscopy (FTIR)

Infrared Spectroscopy techniques have been widely used in studying organic coating for generic identification, surface characterization, coating degradation, and failure analysis (Weldon, 2001). In reality, molecules are constantly undergoing both bending and stretching vibrations. Various molecular vibrations depend primarily on the type of atoms and the type of bonds holding them together, and occur within a relatively narrow range of frequency. The vibrations among the chemical bonds occur at frequencies within the infrared region. If a molecule is exposed to radiation of a frequency exactly matching one of its molecular vibrations, the molecule can adsorb some of this radiation. An infrared spectrum is obtained by focusing an infrared beam through a sample and then observing the frequencies at which the sample adsorbs the radiation (Olsen, 1975; Brezinski, 1991; Suetaka, 1995).

Various experimental set-ups are available in order to acquire IR spectra for materials in form of solid, liquid, gas, or on the surface of metals. Specular reflection, diffuse reflectance, attenuated total reflection, and reflection-adsorption infrared spectroscopy are widely used in surface analysis. Reflection-adsorption infrared spectroscopy (RAIR) has been proved particularly powerful in studying thin film on metal substrates (Williams, 1982; Cheng, 1979; Zhang, 1997). Two types of RAIR are available, namely, near-normal refection-adsorption (NNRA) and grazing angle refection-adsorption (GARA). NNRA IR has an incident angle between 10 to 60^{o}, and is restricted to films in the range of 0.5 to 20 micron. On the other hand, RAIR at near grazing angle ($\sim 80^{o}$) is ideal to study thin films of a few tens of angstroms thick.

1.3.5.3 X-ray Photoelectron Spectroscopy (XPS)

In *X*-ray photoelectron spectroscopy, monoenergetic soft *X*-rays bombard a specimen, causing photoelectrons to be ejected from the surface. The kinetic energy of the photoelectrons can be detected and analyzed with energy analyzer of high resolutions. It is a useful technique for quantitative analysis of surface composition, and offers lateral resolution down to 5 μm and depth resolution to 50 Å. Takeoff angle experiments are useful for studying the interior of thin organic films. The organic film may be etched to certain depths for determination of atomic composition inside the film.

The XPS can detect all elements but hydrogen and helium, which have no core levels.

1.3.5.4 Atomic Force Microscopy (AFM)

In atomic force microscopy (AFM), the sample is scanned past a stationary tip mounted on a microfabricated cantilever. The atoms in the tip interact with these on the surface, resulting in an attractive or repulsive force that deflects the cantilever. A laser beam is used to detect the deflection of the cantilever and record the change of the forces between the tip and the surface. The interatomic forces strongly depend on the separation distance. Thus AFM can be used in mapping of surface topography.

In contrast to scanning tunneling microscopy (STM), AFM can image both conductors and nonconductors with atomic resolution (McClelland, 1987), because it measures the interatomic force between the atom on the surface and the tip instead of the tunneling current. Both techniques are non-destructive. STM has vertical and lateral resolution down to 0.01 Å and atomic scale, respectively, while AFM has vertical and lateral resolution at 0.1 Å and 1 nm, respectively.

1.4 RESEARCH OBJECTIVES

The primary objective of the present investigation is to develop novel chrome-free organic conversion coatings for CRS sheets. These coatings are required to have acceptable corrosion resistance and good paint adhesion. They must be uniform, thin films (<1~2 μm) with pleasant appearance, and with satisfactory electrical properties for grounding and welding.

Various surfactants, including silanes, carboxylates, thiols, xanthates, sulfate, hydroxamates, amine and imidazoles, pyridinium, phosphonic acids, etc., were tested for coating the steel sheets under various conditions. They were subjected to salt spray test for the evaluation of corrosion performance. The promising surfactants were used alone, or in combination with resin that was provided by POSCO. The test results were used to identify the most promising organic coatings for three different substrates, i.e., i) phosphated & galvanized steel, ii) galvanized steel, and iii) untreated bare steel sheet. To date, only the first two samples have been tested and the results will be disclosed in the present report.

1.5 REPORT ORGANIZATION

Three novel coating systems have been developed in the present work. The results will be reported in Chapter 2 to 4. Each chapter consists of an introduction, experimental (samples,

reagents, and test methods), results and discussions, summary and conclusions, and reference sections.

In Chapter 2, carboxylates have been studied for coating phosphated EG steels. The promising surfactants include *10*-undecenoic acid (UA), oleic acid (OA), and other fatty acids such as stearic acids (SA) and palmitic acids (PA). When used alone, they can produce a highly hydrophobic surface and increase the polarization resistance. They can act as a good coupling agent between the phosphate surface and top resin. When subsequently coated with resin, they improve the corrosion resistance significantly as evaluated by salt spray test.

Chapter 3 introduced a nanoscale coating derived from self-assembly monolayers (SAMs) of alkanethiol for both phosphated and EG steels. *1*-Octadecanethiol (ODT) has been used as a model reagent for the formation of SAMs on steel. This CH_3-terminated thiol produces a low surface energy coating that exhibits good corrosion resistance (50~60 hours in SST). It is found that thiols can give the same, in some case, even better corrosion protection than silanes such as VS, and BTSE.

In Chapter 4, HO- and COOH-terminated thiols have been tested on EG steel in order to improve the paintability of thiol coatings. Thiols with functional groups (-OH, -COOH, $-NH_2$, etc.) can produce a higher energy surface, which will provide a good adhesion to topcoats (e.g., resin). Subsequently, the conventional resin has been modified with thiol additives successfully. Evaluated by SST, the corrosion resistance of ODT-modified resin can increase to over 250 hours from 72 hours while without modification. This innovation is very simple, easy to be commercialized. A model has been proposed to explain the mechanism of corrosion protection of thiol-modified resin.

Finally, Conclusions are given in Chapter 5.

REFERENCES

Agarwal, P. and Landolt, D., *Corrosion Sci*., 40, 673-691, **1998**.

Alara, D. L.and Nuzzo, R. G., *Langmuir*, 1, 45, **1985**a.

Alara, D. L.and Nuzzo, R. G., *Langmuir*, 1, 52, **1985**b.

Alsten, J. G., *Langmuir*, 15, 7605-7614, **1999**.

Alves, C. A.; Smith, E. L. and Porter, M. D., *J. Am. Chem. Soc*., 114, 1222, **1992**.

Appleman, B. R. and Campbell, P. G., *J. Coatings Tech*., 54, 17, **1982**.

Appleman, B. R, *J. Protective Coatings & Lining*, 134-143, October **1992**.

Aramaki, K., *Corrosion Sci.*, 41, 1715-1730, **1999**.

Azzaroni, O; Cipollone, M; Vela, M. E. and Salvarezza, R. C., *Langmuir*, 17, 1483-1487, **2001**.

Baboian, R., Corrosion Tests and Standards: Application and Interpretation, 91-97, ASTM, **1995**.

Bain, M.; Troughton, E. B.; Tao, Y. -F.; Evall, J.; Whitesides, G. M. and Nuzzo, R. G., *J. Am. Chem. Soc.*, 111, 321, **1989**a,

Bain, M.; Evall, J. and Whitesides, G. M., *J. Am. Chem. Soc*., 111, 7155, **1989**b.

Bard, A. J. and Faulker, L. R., Electrochem. Methods,103, John Wiley & Sons, New York, **1980**.

Barrena, E.; Ocal, C. and Salmeron, E., *Surface Sci*., 482-485, 1216-1221, **2001**.

Bell, J. P.; Schmidt, R.G.; Malofsky, A. and Mancini, D., *J. Adhesion Sci. Tech*., 5,10, 927-944, **1991**.

Blohowiak, K.Y.; Osborne, J. H. and Krienke, K. A., US Patent No. 5,869,141, Feb. 9, **1998**a.

Blohowiak, K.Y.; Osborne, J. H. and Krienke, K.A., US Patent No. 5,814,137, Sep. 29, **1998**b.

Blohowiak, K.Y.; Osborne, J. H. and Krienke, K. A., US Patent No. 5,849,110, Dec.15, **1998**c.

Blohowiak, K.Y.; Osborne, J. H. and Krienke, K. A., US Patent No. 5,869,140, Feb. 9, **1999**.

Brezinski, D.R.(Ed.), An Infrared Spectroscopy Atlas for the Coatings Industry, Federation of Soc. Coat. Tech., **1991**.

Brown, K., *Finishing*, 38-40, December **1996.**

Butt, H. J.; Seifert, K. and Bamberg, E., *J. Phys. Chem*., 97, 7316, **1993**.

Camillone, N.; Leung, T. Y. B.; Schwartz, P.; Eisenberger, P.; Scoles, G., *Langmuir*, 12, 2737, **1996**.

Castellucci, N. T., US Patent No. 5,206,285, Apr. 27, **1993**a.

Castellucci, N. T., US Patent No. 5,270,428, Dec.14, **1993**b.

Castellucci, N. T., US Patent No. 5,339,748, Aug. 9, **1994**.

Cavalleri, O.; Hirstein, A.; Bucher, J. -P. and Kern, K., *Thin Solid Films*, 284-285, 392-395, **1996**.

Chapman, J. A. and Tabor, D., *Proc. R. Soc*., A 242, 96, **1957**.

Chen, S. H. and Frank, C. F., *Langmuir*, 5, 978, **1989**.

Cheng, S, -Y, Ph.D dissertation, University of Cincinnati, **1979**.

Chidambaran, P. R.; Rangarajan, V. and Van Ooij, W. J., *Surf. Coat. Tech*, 46, 245, **1991**.

Chidsey,C. E. C; Liu, G. -Y; Rowntree, P. and Scoles, G., *J. Phys*. *Chem.*, 91, 4421, **1989**.

Chidsey, C. E. C and Loiacono, D. N., *Langmuir*, 6, 682, **1990**.

Child, T. F. and van Ooij, W. J., *Trans. TMF*, 77(2), 64-70, **1999**.

Comyn, J., in "Structural Adhesives: Developments in Resins and Primers" (A. J. Kinloch, Ed.), Elsever Applied Science, 269-312, **1986**.

Cremer, N. D., Prohesion compared to salt spray and outdoors cyclic method of accelerated corrosion testing, presented at Federation of Soc. Coatings Tech., Paint Show, **1989**.

De Wit, J. H. W., in "Corrosion Mechanism in Theory and Practice" (Marcus, P. and Ouder, J., Ed.), Marcel Dekker, New York, 581-628, **1995**.

Depasquale, R. J. and Evans, J. M., US Patent No. 4,618,688, Oct. 21, **1986**.

Depasquale, R. J. and Evans, J. M., US Patent No. 4,645,846, Feb. 24, **1987**.

Englehart, E. T. and Sowinski, G. Jr., *SAE Journal*, 72, 51, **1974**.

Enick, R. M. and Beckman, E., UN Patent No. 6,183,815 B1, Feb. 6, **2001**.

Fenter, P., in "Thin Film" (A. Ulman, Ed.), 24, 111-147, Academics Press, San Diego, **1998**.

Fenter, P.; Eberhardt, A. and Eisenberger, P., *Science*, 266, 1216, **1994**.

Fenter, P.; Eberhardt, A.; Liang, K. S. and Eisenberger, P., *J. Chem. Phys*., 106, 1660, **1997**.

Ferguson, F. S. and Whitesides, G. M., in "Modern Approaches to Wettability: Theory and Applications", (M. E. Schrader and G. I. Loeb, Ed.), 150-154, **1992**.

Finklea, H. O., *Electroanalytical Methods*, 11, 10090-10115, **2000**.

Folkers, J. P.; Laibinis, P. E.; Whitesides, G. M.; Deutch, J., *J. Phys. Chem*., 98, 563-571, **1994**.

Fousse, D., US Patent No. 5,925,417, **1999**.

Fukushima, H.; Miyashita, S.; Ishida, M.; Holmes, A. and Huck, W., US Patent No. 0164419 A1, Nov.7**, 2002**.

Good, R. J.; Srivates, N. R.; Islam, M.; Huang, H. T. L. and Van Oss, C. J., *J. Adhesion Sci. Tech.*, 4, 8, 607-617, **1990**.

Gothelf, K. V., *J. Electroanalytical Chem*., 494, 147-150, **2000**.

Grundmeier, G.; Reinartz, C.; Rohwerder, M. and Stratmann, M., *Electrochimica Acta*, 43, 1-2,165-174,**1998**.

Hack, H. P. and Scully, J. R., *J. Electrochem. Soc*.,138, 1, 33-40, **1991**.

Halko, D. J. and Halko, B. T., US Patent No. 6,102,521, Aug.15, **2000**.

Hefter, G. T.; North, N. A. and Tan, S. H., *Corrosion*, 53, 8, 657-667, **1997**.

Himmelhaus, M.; Eisert, F.; Buck, M. and Grunze, M., *J. Phys. Chem*., B104, 576, **2000**.

Huang, D. Y. and Tao, Y. -T., *Bull. Inst. Chem., Acad. Sin*., 33, 73, **1986**.

Ishibashi, M.; Itoh, M.; Nishihara, H. and Aramaki, K., *Electrochemica Acta*, 41, 241-248, **1996**.

Ishida, H., in "Adhesion Aspects of Polymeric Coatings" (K.L. Mittal, Ed.), Plenum, New York, 45, **1983**.

Jennings, G. K. and Laibinis, P. E., *Colloids and Surface A: Physicochemical and Engineering Aspects*, 116, 105-114, **1996**.

Jennings, G. K. and Laibinis, P. E., in "Organic Coatings for Corrosion Control", ACS Symposium Series 689, (G. P. Bierwagen, Ed.), 409-419, **1998**.

Karpovich, D. S.; Schessler, H. M. and Blanchard, G. J., in "Thin Film" (A. Ulman, Ed.), 24, 43-79, Academics Press, San Diego, **1998.**

Kendig, M. W.; Mansfeld, F. and Tsai, S., *Corrosion Sci*., 23, 4, 317, **1983**.

Kendig, M. W. and Scully, J. R., *Corrosion*, 46, 1, 22, **1990**.

Kluth, G. J.; Sung, M. M. and Maboudian, R., *Langmuir*, 13, 3775, **1997.**

Kokkoli, E. and Zukoski, C. F., *J. Colloid. Interface Sci*., 209, 60-65, **1999**.

Kubota, T.; Yoshimi, N.; Ando, S.; Matsuzaki, A. and Yamashita, M., Proceedings of SEAISI, Vol.1, Session 10, Tokyo, April **2000**.

Kurth, D. G. and Bein, T., *Langmuir*, 11, 3061-3067, **1995**.

Kuznetsov, Y., Organic Inhibitors of Corrosion of Metals, (Mercer, A. D., Translator; Thomas, J. G. N., Ed.), Plenum Press, New York, **1996**.

Laibinis, P.E.; Palmer, B. J.; Lee, S. -W and Jennings, G. K., in "Thin Film" (A. Ulman, Ed.), 24, 1-41, Academics Press, San Diego, **1998**.

Lee, T. S. and Money, K. L., *Materials Performance*, 23, 28, **1984**.

Leidheiser, H. and Funke, W., *JOCCA*, 121, **1987**.

Leyden, D. E. and Atwater, J. B., *J. Adhesion Sci. Tech*., 5, 10, 815-829, **1991**.

Lin, T. J.; Chun, B. H.; Yasuda, H. K.; Yang, D. J. and Antonelli, T. A., *J. Adhesion Sci. Tech*., 5, 10, 893-904, **1991**.

Mansfeld, F. and Kendig, M. W., "Electrochemical Impedance Tests for Protective Coatings", (C.Haynes and R. Roborian, Ed.), ASTM Publication STP 866, Philadelphia, 122, 1985.

Mansfeld, F.; Kendig, M. W. and Tsao, S., Corrosion, 38, 9, 478, 1982.

McClelland, G. M.; Erlandsson, R. and Chiang, S., Review of Progress in Quantitative Nondestructive Evaluation 6, Plenum: New York, 1987.

McIntyre, J. F.; Claffey, W. J.; Brent, R. J. and Conrad, R., Tri-Service Conference on Corrosion, II, Navel Surface Warfare Center-Carderock Division, 8:30-8:42, **1997**.

Miller, R. N., US Patent No.5,221,371, Jun. 22, **1993**.

Miller, R. N., US Patent No.5,356,492, Oct. 8, **1994**.

Miller, R. N., US Patent No.5,399,210, Mar. 21, **1995**a.

Miller, R. N., US Patent No.5,419,790, May 30, **1995**b.

Miskovic-Stankovic, V. B. and Drazic, D. M., Eurocorr' 96, 34-45, (L. Fedrizzi and P. L. Bonora, Ed.), The Inst. of Materials, **1997**.

Mittal, K. L., Silanes and Other Coupling Agents, V.S.P. Intl Sci., **2001**.

Munger, C. G., Corrosion Prevention by Protective Coatings, NACE, **1984**.

Nishida, N.; Hara, M.; Sasabe, H. and Knoll, W., *Jpn. J. Appl. Phys*., 35, L799, **1996**.

Nozawa, K.; Nishihara, H. and Aramaki, K., *Corrosion Sci*., 39, 9, 1625-1639, **1997**.

Nozawa, K. and Aramaki, K., *Corrosion Sci*., 41, 57-73, **1999**.

Nuzzo, R. G.; Dubois, L. H. and Allara, D. L., *J. Am. Chem. Soc*., 112, 558, **1990**a.

Nuzzo, R. G.; Korenic, E. M.; Dubois, L. H., *J. Phys. Chem*., 93, 767, **1990**b.

Ogawa, H.; Chihera, T. and Taya, K., *J. Am. Chem. Soc*., 107, 1365, **1985**.

Olsen, F., Modern Optical Methods of analysis, McGraw-Hill, **1975**.

Olsen, C-O. A.; Agarwal. P.; Frey, M. and Landolt, D., *Corrosion Sci*., 42, 1197-1211, **2000**.

Page, P.G and E. P. Plueddemann, *J. Adhesion Sci. Tech*., 5, 831-842, **1991**.

Park, G. B.; Kagami, J. P.; Gong, D. C. and Osada, Y., *Thin Solid Films*, 350, 289-294, **1999**.

Petrole, A. P. and Rivera, J. B., US Patent No. 5,700,523, Dec. 23, **1997**.

Petrunin, M.A.; Nazarov, A. P. and Mikhailovski, Y. N., *J. Electrochem. Soc*., 143,1, **1996**.

Pfaum, J.; Bracco, G.; Schreiber, F.; Colorado, R.; Shmakov, O. E.; Lee, T. R.; Scoles, G. and Kahn, A., *Surface Sci*., 498, 89-104, **2002**.

Plueddemann, E. P., Silane Coupling Agents, Plenum, 2nd Edition, **1991**.

Poirier, G. M. and Tarlov, M. J., *Langmuir*, 10, 2853, **1994**.

Porter, M. D.; Bright, T. B.; Allara, D. L. and Cidsey, C. E. D., *J. Am. Chem. Soc*., 109, 3559, **1987**.

Porter, F. C., Corrosion Resistance of Zinc and Zinc Alloys, 88-89, Marcel Dekker, **1994**.

Pu, Z.; van Ooij, W. J. and Mark, J. E., *J. Adhesion Sci. Tech*., 11, 29-47, **1997**.

Puomi, P and Fagerholm, H. M., *Anti-Corrosion Methods and Materials*, 48, 1, 7-17, **2001**.

Quan, Z.; Chen, S. and Li, S., *Corrosion Sci*., 43,1071-1080, **2001**.

Quinton, L. T. and Dastoor, P., *Surface and Interface Analysis*, 25, 931-936, **1997**.

Rocca, E. and Steinmetz, J., *Corrosion Sci*., 43, 891-902, **2001**.

Sabata, A.; Van Ooij, W. J. and Koch, R. J., *J. Adhesion Sci. Tech*., 7, 11, 1153-1170, **1993**.

Sabata, A. and Van Ooij, W. J., US Patent No. 5,326,594, Jul. 5, **1994**.

Sabata, A. and Van Ooij, W. J., US Patent No. 5,478,655, Dec. 26, **1995**.

Sastry, M., *Bull. Mater. Sci*., 23, 3, 159-163, June **2000**.

Scherer, J.; Vogt, M. R.; Magnussen, O. M. and Behm, R. J., *Langmuir*, 13, 7045-7051, **1997**

Schlotter, N. E.; Porter, M. D.; Bright, T. B. and Alara, D. L., *Chem. Phys. Lett*., 132, 93, **1986**.

Schreiber, F.; Eberhardt, A.; Leung, T. Y. B.; Schwartz, P.; Wetter, S. M.; Lavrich, D. J.; Berman, L.; Fenter, P.; Eisenberger, P. and Scoles, G., *Phys. Rev*., B57, 12476, **1998**.

Schreiber, F., *Progress in Surface Sci*., 65, 151-256, **2000**.

Scully, J. R., *J. Electrochem. Soc*., 136, 4, 979, **1989**.

Shih, P. T. K and Koenig, J. L., *Mater. Sci. Eng.*, 20, 137, **1975**.

Shuford, D. M., US Patent No. 5,326,595, Jul. 12, **1994**.

Shulman, G. P., and Bauman, A. J., Environmentally Acceptable Inhibitors and Coatings, Electrochemical Society Inc., 196-201, **1997**.

Simpson, C. H.; Ray, C. J. and Skerry, B. S., *J. Protective Coatings & Lining*, May **1991**.

Skerry, B. S. and Simpson, C. H., NACE Corrosion Conference, Paper 412, Cincinnati, **1991**.

Smart, M. G.; Brown, C. A. and Gordon, J. D., *Langmuir*, 9, 1082, **1993**.

Stevens, M. J., *Langmuir*, 15, 8, 2773-2778, **1999**.

Stratmann, M.; Furbeth, W.; Grundmeier, G; Losch, R and Reinartz, C. R., in "Corrosion Mechanism in Theory and Practice", (Marcus, P. and Ouder, J., Ed.), Marcel Dekker, New York, 373-419, **1995**.

Strong, L. and Whitesides, G. M., *Langmuir*, 4, 546, **1988**.

Suetaka,W., Surface Infrared and Raman Spectroscopy: Methods and Application, Plenum, New York, **1995**.

Sung, M. M. and Kim, Y., *Bull. Korean Chem. Soc*., 22, 748-752, **2001**.

Tait, W. S., An Introduction to Electrochemical Corrosion Testing for Practicing Engineers and Scientists, Pair O Docs Publications, Racine, Wisconsin, **1994**.

Taneichi, D.; Haneda, R. and Aramaki, K., *Corrosion Sci*., 43, 1589-1600, **2001**.

Tang, Nie and van Ooij, W. J., *Progress in Organic Coatings*, 30, 4, 255-263, **1997**.

Tesoro, G. and Wu, Y., *J. Adhesion Sci. Tech*., 5, 771-784, **1991**.

Tillman, N.; Ulman, A.; Schildkraut, J. S. and Penner, T. L., *J. Am. Chem. Soc*., 110, 6136, **1988**.

Timmins, F. G., *J. Oil Color Chem. Assoc*., 62, 131, **1989**.

Tredgold, R. H., Order in Thin Organic Films, Cambridge University Press, **1994**.

Troughton, E. B.; Bain, C. D.; Whitesides, G. M.; Nuzzo, R. G.; Allara, D. L. and Porter, M. D., *Langmuir*, 4, 365, **1988**.

Truong, K. D. and Rowntree, P. A., *J. Phys. Chem*., 100, 19,917, **1995**.

Ulman, A., An Introduction to Ultrathin Organic Films: From Langmuir-Blodgett to Self-Assembly, Academic Press, San Diego, **1991**.

Ulman, A., *Chem. Review*, 96, 1533-1554, **1996**a.

Ulman, A., *Thin Solid Films*, 273, 48-53, **1996**b.

Van Eijnsbergen, J. F. H., Duplex System, Elsevier, **1994**.

Van Ooij, W. J.; Leijenaar, S. L. and Van den Burgh, B., XVI FATIPEC Congr. 56, **1982**a.

Van Ooij, W. J. and Sabata, A., *J. Adhesion Sci. Tech*., 5, 10, 843-963, **1991**.

Van Ooij, W. J. and Sabata, A., US Patent No. 5,208,793, Apr. 28, **1992**.

Van Ooij, W. J. and Sabata, A., US Patent No. 5,200,275, Apr. 6, **1993**a.

Van Ooij, W. J.; Edwards, R. A.; Sabata, A. and Zappia, J., *J. Adhesion Sci. Tech*., 7, 897-917, **1993**b.

Van Ooij, W. J. and Sabata, A., *Surface and Interface Analysis*, 20, 457-484, **1993**c.

Van Ooij, W. J.; Edards, R. A. and Sabata, A., US Patent No. 5,292,549, Mar. 8, **1994**a.

Van Ooij, W. J. and Sabata, A., US Patent No. 5,322,713, Jun. 21, **1994**b.

Van Ooij, W. J. and Sabata, A., US Patent No. 5,433,976, Jul. 18, **1995**a.

Van Ooij, W. J., US Patent No. 5,455,080, Oct. 3, **1995**b.

Van Ooij, W. J., US Patent No. 5,498,481, Mar. 3, **1996**a.

Van Ooij, W. J., US Patent No. 5,539,031, Jul. 23, **1996**b.

Van Ooij, W. J.; Subramanian, V. and Zhang, C., US Patent No. 5,750,197, May 12, **1998**a.

Van Ooij, W. J., and Yuan, W., US Patent No. 5,759,629, Jun.2, **1998**b.

Van Ooij, W. J. and Child, T. F., *Chemtech*, 26-35, Feb. **1998**.

Van Ooij, W.J.; Subramanian, V. and Zhang, C., US Patent No. 6,261,638 B1, Jul.17, **2001**.

Van Ooij, W. J., Corrosion Control of Metals by Organic Coatings, CRC Press, **2003**.

Van Oss, C. J., Interfacial Forces in Aqueous Media, Marcel Dekker, New York, **1994**.

Volmer, M., Ph.D dissertation, University of Dortmund, **1989**.

Walker, P., in "Surface Coatings", 1, (Ed ., A. D. Wilson), Elsever Applied Sci., 191, **1987**.

Weldon, D.G., Failure Analysis of Paints & Coat.,231-233, John Wiley & Sons, New York, **2001**.

Wicks, Z. W.; Jones, F. N. and Pappas, S. P., *Organic Coatings: Sci. & Tech*., Vol. II, 153-169, John Wiley & Sons, New York, **1994.**

Wiederholt, W., The Chemical Surface Treatment of Metals, (W. E. Cattley, Ed., English Translation), Robert Draper Ltd., **1965**.

Williams, J. W., Ph.D dissertation, University of Cincinnati, **1982**.

Yuan, W. and van Ooij, W. J., *J. Colloid & Interface Sci*., 185, 197-209, **1997**.

Zamborini, F. P. and Crooks, R. M., *Langmuir*, 14, 3279-3286, **1998**.

Zerulla, D.; Uhlig, I.; Szargan, R. and Chasse, T., *Surface Sci*., 402-404, 604-608, **1998**.

Zhang, C., Ph.D dissertation, University of Cincinnati, **1997**.

Zhou, H.; Lu, W; Yu, S. and He, P., *Langmuir*, 16, 2797-2801, **2000**.